Global and Planetary Change 172 (2019) 15–32

Contents lists available at ScienceDirect

Global and Planetary Change

journal homepage: www.elsevier.com/locate/gloplacha

Hot-house climate during the Triassic/Jurassic transition: The evidence of climate change from the southern hemisphere (Salt Range, Pakistan)

Shahid Iqbal[a,b,*], Michael Wagreich[b], Jan Irfan U[c], Wolfram Michael Kuerschner[d], Susanne Gier[b], Mehwish Bibi[b]

[a] Department of Earth Sciences, Quaid-i-Azam University Islamabad, Islamabad 45320, Pakistan
[b] Department for Geodynamics and Sedimentology, University of Vienna, Althanstrasse 14, Vienna A-1090, Austria
[c] National Centre for Excellence in Geology, University of Peshawar, Peshawar 25130, Khyber Pakhtunkhwa, Pakistan
[d] Department of Geosciences, University of Oslo, 1047 Blindern, 0316, Oslo, Norway

ARTICLE INFO

Keywords:
GreenhoTriassic–Jurassic boundary
Pakistan
Geochemistry
Clay mineralogy

ABSTRACT

The Triassic–Jurassic boundary interval was characterised by the change from warm, semiarid–arid to a hot and humid climate in the Tethyan domain linked to input of greenhouse gases from the Central Atlantic Magmatic Province (CAMP) activity and Pangaea breakup. This study provides the very first outcrop evidences of palaeoclimatic evolution during the Triassic–Jurassic boundary interval in the then southern hemisphere, along the eastern margin of Gondwana facing the western Tethys. In the Tethyan Salt Range of Pakistan a succession of Upper Triassic dolomites, green-black shales (Kingriali Formation) to overlying Lower Jurassic quartzose sandstones, shales, laterites and conglomerates (Datta Formation) represents the sedimentary archives of this critical time interval. Bulk and clay mineralogy of the Upper Triassic shales indicate the presence of mainly illite while kaolinite is a minor component. The kaolinite content, a reflection of the mature stage of chemical weathering and hence hot–humid conditions, increases up-section in the overlying shales and sandstone–shale succession. The following laterite–bauxite horizons lack illite and are entirely composed of kaolinite, boehmite and haematite. The bulk rock geochemistry of the succession confirms a similar trend. The Chemical Index of Alteration (CIA_{molar}) displays an increasing trend from the Upper Triassic (CIA 68–80) to the overlying Lower Jurassic strata (CIA 90–97). The overall results for the succession reveal an increasing chemical maturity trend from Rhaetian to Hettangian thereby supporting a change from warm-arid to a hot and humid palaeoclimate, probably extreme greenhouse conditions. Similar changes in the clay mineralogy and sediment geochemistry across the Triassic–Jurassic boundary have been reported from basins across Europe. Thus the Salt Range provides sections from the southern hemisphere for correlations across the Triassic–Jurassic boundary.

1. Introduction

The Phanerozoic palaeoclimatic fluctuations (Poulsen, 2009) had a variety of temporal scales and a wide range of climatic states, with “greenhouse” and “icehouse” phases, and hothouse and glacials as extreme end members (Kidder and Worsley, 2010). Climate proxy data (e.g. Frakes, 1979; Crowley and North, 1991; Frakes et al., 1992; Allen et al., 1994; Valdes et al., 1999; Huber et al., 2000) over the past 500 Ma, provide vast evidences suggesting that the Earth has been generally warmer than at present.

The Mesozoic Earth, in comparison to the present day, was warmer by 6 °C or more (Sellwood and Valdes, 2006). Modeling of the Late Triassic evaporation and precipitation data indicate a warm semiarid to arid palaeoworld (Simms and Ruffell, 1989; Therrien and Fastovsky, 2000; Whiteside et al., 2011). In the Tethyan domain, the Late Triassic was dominated by warm, semiarid to arid climatic conditions (Hornung et al., 2007; Arche and López-Gómez, 2014) with two short-lived relatively wet peaks during the middle-late Carnian known as the Carnian Pluvial Event (Dal Corso et al., 2012; Ruffell et al., 2016; López-Gómez et al., 2017). Afterwards, arid conditions established and the Late Triassic has so far not yielded any evidence of glacial activity, making it a unique period in the Earth's Phanerozoic history (Preto et al., 2010).

In the Tethys realm the Early Jurassic marks a change from a dominantly warm-arid to a more humid palaeoclimate (Kuerschner

* Corresponding author at: Center for Earth Sciences, Department of Geodynamics and Sedimentology, UZA II - Universitätszentrum Althanstrasse 14, A-1090 Vienna, Austria.
E-mail address: siqbal_geol@yahoo.com (S. Iqbal).

https://doi.org/10.1016/j.gloplacha.2018.09.008
Received 14 February 2018; Received in revised form 17 September 2018; Accepted 17 September 2018
Available online 21 September 2018
0921-8181/ © 2018 Elsevier B.V. All rights reserved.

et al., 2007; Ruckwied and Götz, 2009; Bonis and Kürschner, 2012), globally correlated with the voluminus basaltic (LIP) volcanic activity of the Central Atlantic Magmatic Province (CAMP) at the Triassic–Jurassic boundary (Marzoli et al., 1999, 2004; Pálfy et al., 2000; Wignall, 2001; Hesselbo et al., 2002). The CAMP activity is associated with the Pangaea rifting and is considered as a favored trigger for extreme warming via greenhouse gas exhalation responsible for the Triassic/Jurassic mass extinction (Olsen, 1999; Pálfy et al., 2001; Ruhl et al., 2011a,b).

In the then southern hemisphere, the Karoo-Ferrar Continental Flood Basalt (CFB) emplacement is linked to the Early Jurassic break-up of Gondwana (Duncan et al., 1997; Pálfy et al., 1997; Pálfy and Smith, 2000) and caused oceanic anoxia (Hallam, 1987; Jenkyns, 1999) and global warming (Hesselbo et al., 2000). This CFB emplacement may have played an important role in shaping the Early Jurassic margins of the associated plates, including the northwestern margin of the Indian plate, thereby controlling the large-scale geometries of the Lower Jurassic siliciclastic depositional systems in the region.

The tectonic activities at the Triassic–Jurassic boundary and the Early Jurassic played important role in controlling the relative sea-level fluctuation during this time interval. A short lived but pronounced sea-level fall has been reported in different parts of the world during this interval (Haq et al., 1987; Hallam, 1988, 1997, 2001; Hallam and Wignall, 1999; Haq, 2017). This sea-level fall may have exposed new areas to the greenhouse climate thereby substantially enhancing magnitude and extend of chemical weathering in these areas.

The palaeoclimatic variation and sea-level fall at the Triassic–Jurassic boundary has resulted in a pronounced regression and the deposition of quartz-rich siliciclastics (mostly Lower Jurassic) on top of the exposed, dissolved and reworked Triassic platform carbonates in many European basins (Hesselbo et al., 2004; Haas and Tardy-Filácz, 2004; Letourneau and Huber, 2006), Iran and adjoining Afghanistan (Klett et al., 2006; Fürsich et al., 2009; Wilmsen et al., 2009) Western Australia, Madagascar and India (Mukhopadhyay et al., 2010).

In the Salt and Trans–Indus Ranges, Pakistan (Fig. 1), a thick succession of Lower Jurassic fluvio-deltaic quartz-rich siliciclastics with some shale and carbonates overly Upper Triassic platform carbonates (Iqbal et al., 2014, 2015a, 2015b). The present paper aims to interpret the palaeoclimatic conditions in the Salt and Trans–Indus Ranges (Fig. 1), Pakistan, during the Triassic–Jurassic transition and the Early Jurassic using field evidences, petrographic data, bulk mineralogy, clay mineralogy and sediment geochemistry proxies. Based on this first detailed record from the southern hemisphere, a general regional and global correlation is envisaged to establish the palaeoclimatic context of the succession. This may open a new view from the Gondwana domain in the palaeoclimatic reconstructions for a critical interval of Earth history.

2. Geological setting and palaeogeography

The Salt and Trans–Indus Ranges in Pakistan mark the southern boundary of the Kohat–Potwar Plateau (Fig. 1). The latter unit forms part of the foreland zone of the Himalayan Fold and Thrust Belt (HFTB) and preserves thick Precambrian to Recent sediments (e.g., Shah, 2009). Stratigraphy, structural geology and tectonics have remained the subjects of many studies (e.g. Molnar and Tapponnier, 1981; Hallam and Maynard, 1987; Baker et al., 1988; Burbank and Raynolds, 1988; Davis and Lillie, 1994; Kadri, 1995; Kazmi and Jan, 1997; Jadoon et al., 1997; Shah, 2009; Mohadjer et al., 2010; Jain, 2014; Iqbal et al., 2014; Hanif et al., 2014).

The succession studied includes the Kingriali and Datta formations with a total thickness of 152–270 m. The Upper Triassic Kingriali Formation was named after the Kingriali Peak in the Khisor Range (Gee, 1945). A Late Triassic, Rhaetian age is confirmed by new palynology data, i.e. the presence of the dinoflagellate cysts *Rhaetogonyaulax*, *Suessia* and *Beaumontella* (Kuerschner et al., 2017). The uppermost, shaly part correlates to an extinction event (?) (Kuerschner et al., 2017). The formation conformably overlies the Chak Jabbi Limestone (Middle Triassic) in the Kala Chitta area and has conformable lower contact with the Tredian Formation (Middle Triassic) in all other localities. The upper contact is conformable to the Datta Formation (Iqbal et al., 2017).

The Lower Jurassic Datta Formation was named after the Datta Nala in Surghar Range (Danilchik, 1961; Danilchik and Shah, 1967). It's mainly Hettangian age was recently confirmed by Kuerschner et al. (2017). The formation is predominantly of continental origin (Fatmi, 1977). It is conformably overlain by Shinawari Formation (Toarcian).

Palaeogeographically, the Salt Range was located on the northwestern passive margin of the Indian Plate in the southwestern Tethyan realm, i.e., ~20^{O} - 25^{O} S latitude during Late Triassic–Early Jurassic (Rees et al., 1999, 2002; Damborenea, 2002; Arias, 2007; Fig. 1a). Rifting within the Pangaea during the Triassic–Jurassic boundary interval resulted in the breakup of the Indian Plate from Africa and Arabia and a change in palaeoclimate. The tectonic activity associated controlled the subsidence of the west–northwestward basinal area that is now the Salt Range–Kohat–Potwar Plateau (Fig. 1b, c), and the subsequent development of a large fluvial system, which resulted in the deposition of the Datta Formation on ca. 15,000 Km^2 area (Iqbal et al., 2015b).

3. Material and methods

3.1. Fieldwork and sampling

The upper part of the Kingriali Formation and the entire Datta Formation were studied in the Salt and Trans–Indus Ranges (Fig. 1b, c). Detailed sections were measured at a ca. 300 km transect from Kasanwala, Kaowaali, Nammal Gorge, Zaluch Nala (western Salt Range), Chichali Nala, Gulla Khel, Baroch Nala (Surghar Range) and the Paniala anticline (Khisor Range).

Sedimentological analyses were conducted in the field (Fig. 3) including observation of the vertical and lateral facies variation, sedimentary structures and features following standard sedimentology procedures (e.g. Nichols, 2000; Reading, 2009). Marker horizons such as erosional surfaces, oxidised zones, palaeosols, rippled and cross bedded horizons and beds with plant remains were identified (Fig. 3). In total 400 archived samples were collected covering the entire facies variations (Selley, 2000).

3.2. Petrographic studies

With the exception of loose shales, 300 thin sections were prepared for all the siltstone, sandstone, conglomerates, carbonates and evaporites samples at the Department of Geodynamics and Sedimentology, University of Vienna thin section petrography lab. These thin sections were studied systematically using Leica DM2700 P microscope with Leica MC170 HD camera. Herein, the petrographic studies were focused on sandstones thin section point counting (e.g. Dickinson, 1970; Graham et al., 1976; Appendix. 1) and its application for the interpretation of palaeoclimate and weathering trend.

Petrographically, quartz was subdivided into monocrystalline (Q_m) and polycrystalline (Q_p). The latter also include chert (Ingersoll et al., 1984). The Q_m was subdivided into Q_m with unit extinction (Q_{mue}) and Q_m with undulose extinction (Q_{muu}) (Fig. 4c, e). Similarly the Q_p was subdivided into Q_p (Fig. 4f) with 2–3 crystals ($Q_{pq(2-3)}$) and Q_p with > 3 crystals ($Q_{pq>3}$). The feldspars were subdivided into plagioclase (P) and K-feldspar (A) whereas the lithic fragments were referred to as lithic fragments (L).

The data was plotted on Quartz–Feldspars–Lithic Fragments (QFL) plot (Gazzi, 1966; Gazzi et al., 1973; Dickinson and Suczek, 1979). To follow the practice of the existing literature (e.g. Suttner and Dutta, 1986) R is used and it has the same meaning as L (Ingersoll et al., 1984).

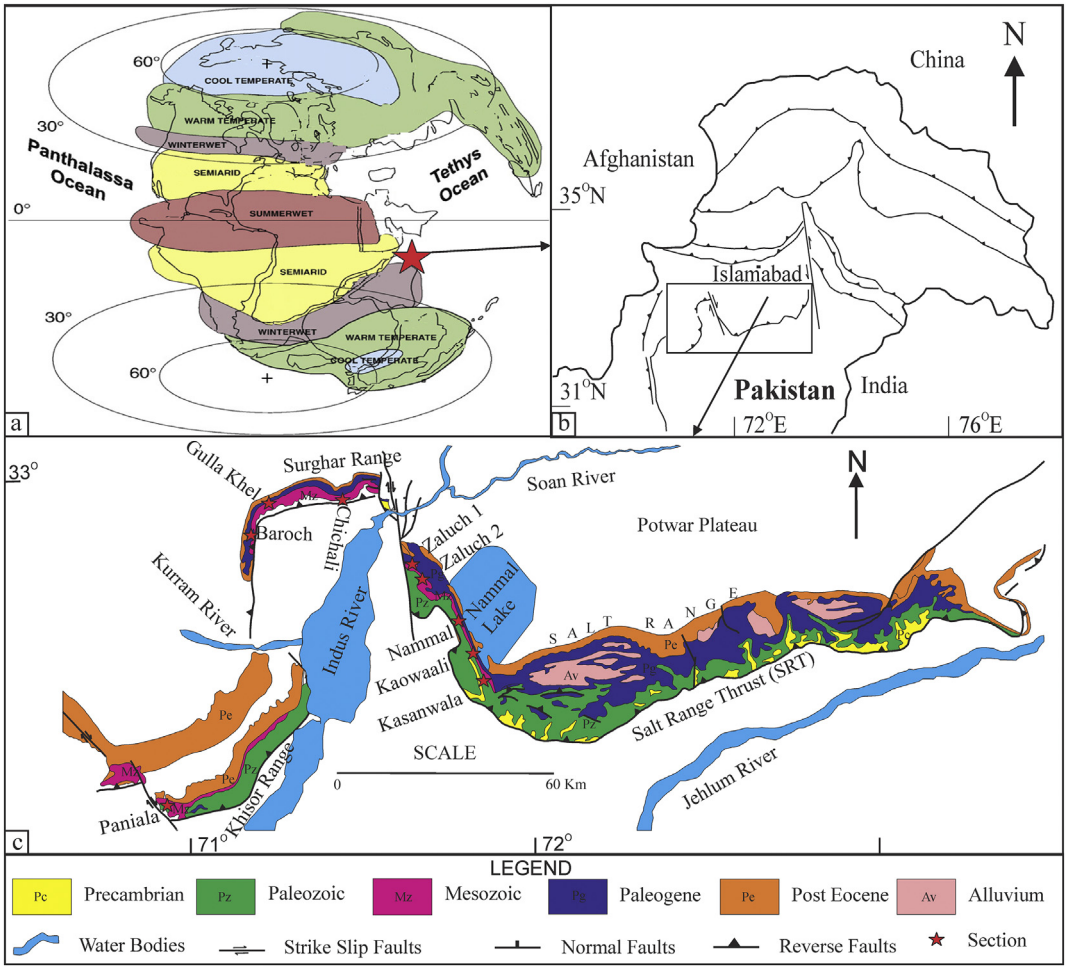

Fig. 1. Current and palaeogeographic location of the Salt Range, Pakistan. (a) Early Jurassic palaeogeographic location of the study area. (b) Tectonic map of north Pakistan with the location of Salt Range–Kohat–Potwar Plateau. (c) Salt and Trans–Indus Ranges with locations of the studied sections (modified after Rees et al., 2000; Iqbal et al., 2015b).

Furthermore, log/log plots for $Q_p/(F + R)$ Vs. $(Q_m + Q_p)/(F + R)$ were used to reconstruct palaeoclimate trends (Suttner and Dutta, 1986). The minimum (F + R) value was fixed as 1 to avoid out scale values (Fig. 5).

3.3. Bulk mineralogy/XRD analysis

Based on fieldwork observations and petrographic analysis, 100 samples were selected for XRD analysis. Powder XRD was used for the determination of the bulk mineralogical composition (Appendix. 2a). XRD analysis was conducted using PANalytical X'Pert Pro diffractometer (CuKα- radiation (40 kV, 40 mA), step size 0.0167, 5 s per step) at the Department of Geodynamics and Sedimentology, University of Vienna.

3.4. Clay mineralogy/XRD separation

30 samples were investigated for clay mineralogy. The samples were treated with hydrogenperoxide (H_2O_2) to remove the organic matter/carbon (Van Langeveld et al., 1978; Mikutta et al., 2005). Following the organic content removal, the samples were dispersed with a 400 W ultrasonic probe. The < 2 μm fraction was separated using Atterberg cylinders. Oriented clay samples were prepared by pipetting 1 ml of suspension (10 mg/ml) onto a glass slide. XRD mounts were analysed, saturated with Mg and K ions and after saturated with glycerol (Mg-samples) and ethylene-glycol (K-samples) to separate smectite and vermiculite. Finally, the samples were heated to 550 °C (Moore and Reynolds, 1997). The XRD patterns (Appendix 2b) were interpreted (Brindley and Brown, 1980; Moore and Reynolds (1997), and quantified using the correction factors (Schultz, 1964).

3.5. Bulk geochemistry

Various geochemical proxies have reliable palaeoclimatic and palaeoenvironmental significance (e.g. Climap, 1976; Nesbitt and Young, 1982; Roser and Korsch, 1988; Wefer et al., 1999; Hofmann et al., 2001; Zachos et al., 2001; Cullers, 2002; De Caritat et al., 2012; Fischer and Wefer, 2012). In the present case 150 samples were powdered and homogenised for bulk rock geochemistry (Appendix 3). The bulk rock geochemistry analyses were conducted in Bureau Veritas Ltd (former Acme) Analytical Laboratories Canada using Inductively Coupled Plasma Emission Spectroscopy/Mass Spectrometry (ICP- ES/MS). The analyses include oxides, major, minor, trace and rare earth elements.

The bulk geochemical composition of the samples was measured using a combination of fusion and Aqua Regia digestion on sample splits. A split of 0.2 mg powdered and homogenised sample was fused in Lithium metaborate/tetraborate followed by Nitric acid digestion to extract Si, Nb, and Rb and measured by Inductively Coupled Plasma Optical Emission Spectrometry (ICP-OES; Spectro Ciros Vision). In addition 0.5 g sample was digested in 95 °C Aqua Regia and analysed for Al, Fe, Mg, Ca, Na, K, Ti, P, Mn, Cr, Ba, Co, Sr, Th, U, V, W, and Zr by ICP-MS (Perkin Elmer ELAN 9000, Sciex). Both splits were calibrated against reference materials SO18, DS 10, and OREAS 45 EA. Total C

(TOT/C) and total S (TOT/S) were detected by LECO analysis. 13 samples were analysed in duplicates. The average analytical error in the analysis is 0.18%.

3.5.1. Geochemical proxies

3.5.1.1. Chemical index of alteration (CIA). The Chemical Index of Alteration (CIA) is a useful proxy for palaeoclimate reconstructions (Yan et al., 2010) and is calculated (Eq. 1; Nesbitt and Young, 1982, 1989; Taylor and McLennan, 1985):

$$CIA_{(molar)} = \left[\frac{Al_2O_{3(molar)}}{Al_2O_{3(molar)} + CaO^*_{(molar)} + Na_2O_{(molar)} + K_2O_{(molar)}} \right] \times 100 \quad (1)$$

Here the CaO* is the amount of CaO incorporated in the silicate fraction of the rock (Nesbitt and Young, 1982; McLennan et al., 1993). Further, all the quantities were used in molar proportions. To avoid errors derived from the unknown CaO content of the silicate fraction, the Chemical Proxy of Alteration (CPA) is used (Eq. 2; Buggle et al., 2011).

$$CPA_{(molar)} = \left[\frac{Al_2O_{3(molar)}}{Al_2O_{3(molar)} + Na_2O_{(molar)}} \right] \times 100 \quad (2)$$

3.5.1.2. Al_2O_3 vs. CIA and K_2O/ Na_2O vs. CIA plots. Al_2O_3 vs. $CIA_{(molar)}$ plot and K_2O/Na_2O vs. $CIA_{(molar)}$ plots are used to differentiate between the arid, subtropical and tropical palaeoclimates (Goldberg and Humayun, 2010). The $CIA_{(molar)}$ in these plots was modified to:

$$CIA_{(molar)} = \left[\frac{Al_2O_{3(molar)}}{CaO^*_{(molar)} + Na_2O_{(molar)} + K_2O_{(molar)}} \right] \quad (3)$$

This modified CIA, a proportion between alumina and alkalis plus calcium, provides a more sensitive indicator of the degree of chemical weathering, as now the values are not restricted to < 100 and the equation (Eq. 3) yields values of > 100 and even up to 500 for laterites (Goldberg and Humayun, 2010).

3.5.1.3. A-CN-K plot. Ternary plot of Al_2O_3, CaO* + Na_2O, and K_2O defines an equilateral triangle called A-CN-K diagram (Nesbitt and Young, 1984; Bahlburg and Dobrzinski, 2011). The diagram explains the linkage between the weathering trends and mineralogical compositions (Basu, 1976). Similarly the positions of smectite, illite, gibbsite, chlorite and kaolinite are indicated (Nesbitt et al., 1996).

3.5.1.4. Chemical maturity proxy plot. Compositional variations play strong role in controlling the amount of Al, Si, K and Na in sediments (Hofmann et al., 2001). Therefore, a bivariant plot of SiO_2 against total $Al_2O_3 + K_2O + Na_2O$ is generally used to represent the chemical maturity trend in the siliciclastic sediments (Suttner and Dutta, 1986; Malick and Ishiga, 2016). The chemical maturity trend is related to the palaeoclimatic conditions during the sedimentation.

4. Results

4.1. Outcrop/field data

The Kingriali Formation consists mainly of light gray, yellowish gray, thick bedded dolomite, and shows only slightly variable thicknesses from the western Salt Range (75 m – 85 m) to the Surghar Range (92 m – 108 m) and the Kala Chitta Range (91 m). The dolomite displays fragmental texture (due to surficial weathering) and is oolitic at places. Very thin beds of dark green, brownish black shale appear in the upper part. Both the occurrence frequency and thickness of the shale beds increase upsection (Fig. 3a). Further upsection, the shale is interbedded with marl and argillaceous dolomite. Dolomite with reworked clasts (Fig. 3b) and fossiliferous horizons (mostly bivalves, gastropods and ostracods) occurs in the uppermost part at western Salt Range. In the uppermost part of the Kingriali Formation at Nammal Gorge and Panaila anticline a conspicuous 30–70 cm shale occurs that includes a 2–15 cm gypsum bed (Fig. 3c, d). This unit overlies a 30 cm rusty brown, haematitic/limonitic dolomite and marks the contact of the Kingriali Formation with the overlying Datta Formation (Fig. 3c).

In the western Salt Range (except the Nammal Gorge) the formation is overlain by a 30–50 m thick succession of white, light gray, rusty brown fine to medium grained sandstones interbedded with red/maroon, orange, gray shale. This lithofacies is overlain by a 8–21 m thick laterite/bauxite (Fig. 3e). This laterite/bauxite is overlain by the conglomerates/pebbly sandstones of the Datta Formation in all the three sections (Fig. 3d).

The thickness of the Datta Formation varies from 132 to 240 m along the transect from the western Salt Range (132 m – 200 m) to the Surghar Range (150 m – 240 m), and the Khisor Range (140 m). The lower part of the Datta Formation consists of conglomerates, pebbly and coarse sandstones of the CBFA (Iqbal et al., 2015b) in the western Salt Range (Fig. 3e). The sandstones and conglomerates are well sorted, rounded and rich in quartz. In the Gulla Khel and Paniala anticline sections the conglomerates do not exist and coarse grained, white sandstone directly overlies the Kingriali Formation. Petrified wood, thin coal patches and reworked coal/wood clasts occur (Fig. 3f).

These are overlain by red-brown sandstones, siltstones and shale of the CMOBFA (Iqbal et al., 2015b). The lower bedding planes are erosive while palaeosol horizons and plant remains occur. Mud cracks, ripples marks and bioturbation features are common.

The LFA consist of brown - black shale and associated carbonates (Iqbal et al., 2015b). The shale is carbonaceous at places while the carbonates include both pure and arenaceous dolomite. Ripple marks and bioturbation are common. Apart from some bivalves and gastropods at Zaluch Nala no fossils were observed in the succession.

4.2. Framework composition/petrographic studies

Of the 300 analysed samples, most are sandstones while carbonates constitute a minor proportion. Thorough dolomitisation and lack of fossil content in the carbonate samples limit their applicability for palaeoenvironmental reconstructions. In the upper part of the formation the dolomites show fragmental texture and clasts alignment (Fig. 3b). Fossiliferous horizons with bivalves, gastropods and ostracods occur in the uppermost part at Kasanwala (Fig. 4a, b) and lamination resembling stromatolites occur.

Quartz is the most common component of sandstones and the total quartz (Q_{total}) averages 95.5% of the framework components. Q_{mue} predominates averaging 76.1% followed by Q_{muu} (12.5%), whereas, $Q_{pq(2-3)}$ content averages 4.3% and $Q_{pq>3}$ averages 2.6% of the bulk framework composition (Appendix 1). High Q_{muu} and Q_P contents occur in the coarse/pebbly sandstones and conglomerates of the CBFA (Iqbal et al., 2015b). The total feldspars (F_{total}) content average only 0.15% of the bulk framework, which are highly decomposed and altered to clay minerals. Very minor potassium feldspar (K) occurs (average 0.13%) while plagioclase feldspar (F) is rare (average 0.02%). The total lithic fragments (L) constitute a minor component, averaging 1.2%. L is the combination of sedimentary lithics (L_s), metamorphic (L_m) and volcanic-hypabysssal (L_v). The QFL plot indicates a cluster of samples near the quartz apex (Fig. 5a). The framework composition comparison, a function of the ratios of grain types and the most sensitive climatic control, is a bivariant log/log plot based on $Q_P/(F + R)$ vs. $Q_{total}/(F + R)$ ratios and displays closely clustered sample populations in the humid zone (Fig. 5b).

4.3. Bulk mineralogy/XRD

The XRD analysis indicates the qualitative mineralogy of the

selected horizons (Appendix. 2a). The upper part of the Triassic carbonates is composed of dolomite and calcite. In the shale unit, in the upper part, the carbonate content decreases and quartz and clay minerals appear. Further up section at the contact with the overlying Jurassic strata the carbonate content disappears and evaporites (gypsum) appear. In the associated shales, illite is the dominant clay mineral. These shales are overlain by laterite horizons rich in kaolinite-haematite. The kaolinite content within these laterites increases upsection and the upper part of the laterite at the Kasanwala section is entirely composed of boehmite. Upsection in all the measured sections, the coarse siliciclastics (CBFA) are quartz rich, while the associated shales with palaeosols (CMOFA) have kaolinite and quartz. The overlying shales of the LFA are composed of clay minerals, quartz and carbonates with an increasing carbonate (dolomite and ankerite) content trend upsection. Kaolinite is the dominant clay mineral but the illite content increases upsection.

4.4. Clay mineralogy

Clay mineralogy indicates the presence of a simple mixture of illite and kaolinite (Appendix. 2b). In the Kingriali Formation, illite is by far the dominant clay mineral, averaging 94.1% while the remaining 5.9% is kaolinite. The lower part of the Triassic strata indicates kaolinite as a minor component that completely disappears in the green shales.

In the overlying Datta Formation kaolinite is the dominant clay mineral, averaging 68.5% of the total clays, while the remaining 31.5% is illite. Following the very low kaolinite content during the Triassic a jump to very high kaolinite is observed at the end of the Triassic. The highest kaolinite content is present in the CMOFA (92.2%) whereas, the lowest content occurs in the LFA (37.2%). The laterite/bauxite horizons are kaolinite rich.

4.5. Bulk geochemistry

4.5.1. Chemical index of alteration (CIA)

The CIA (molar) plots (Figs. 2b, 7) display low values for the Triassic strata (shales) ranging 68.5–80 averaging 77.7. The CIA has a mean of 92.7 for the Jurassic strata with the Kasanwala and Gulla Khel section displaying the highest average values of 94.9 and 94.6 respectively while the Nammal Gorge section has the lowest average of 88.8. Stratigraphically, the coarse grained sandstones-conglomerates (CBFA) and the associated laterites/palaeosols possess the highest CIA values generally over 95. Exceptionally high values of 99.8 are calculated for the uppermost part of the thick laterites at the Kasanwala.

After the continuous high CIA values in the CBFA, a gradual drop in the CIA value is observed through the CMOFA to the LFA (Fig. 2b). However, the CIA values are still above 85 in this interval. After this interval of relatively low CIA values, the overlying sandstones (second repetition of CBFA) again display high CIA values (mostly above 90) before another drop but still > 80 corresponding to the second repetition of the LFA. This second fluctuation corresponds to the second depositional sequence interpreted by Iqbal et al. (2015b).

In order to verify the validity of the CIA, CPA (Buggle et al., 2011) was used, giving an average value of 98.8 for the Triassic strata with a minimum value of 96.2. For the Jurassic strata the CPA yields an average of 99 with a minimum value of 97.

4.5.2. Al_2O_3 vs. CIA and K_2O/Na_2O vs. CIA Plots

The Al_2O_3 vs. $CIA_{(molar)}$ plot for the Kingriali Formation indicates a cluster of samples in the $CIA_{(molar)}$ range 1–2 and Al_2O_3 range of 7–25 (Fig. 6a). A gradual upsection increase in the Al_2O_3 content is observed. In the lower part of the succession the Al_2O_3 content increases upwards (up to 15% Al_2O_3) with no prominent change in the CIA. The boundary beds can be easily differentiated from the rest due to a distinct increase in both the Al_2O_3 and CIA (Fig. 6a).

All samples of the Datta Formation plot to the right of the Triassic samples and have 0–40 range for Al_2O_3 (Fig. 6a). The highest CIA and Al_2O_3 are plotted for the laterite/bauxite samples. The CBFA and sandstone-siltstone of the CMOFA display higher CIA values but the Al_2O_3 content is mostly below 15%. The lowest Al_2O_3 accompanied by relatively low CIA values correspond to the floodplain siltstone of the CMOFA while the associated palaeosols in the COMFA still plot in the high CIA and Al_2O_3 rich part. This allows their differentiation from the shales of the LFA which plot in the zone of relatively high Al_2O_3 but comparatively low CIA. The second depositional sequence displays a similar trend.

The K_2O/Na_2O vs. CIA Plot displays a wide range for the K_2O/Na_2O in the Kingriali Formation (Figs. 6b). The lowest K_2O/Na_2O ratios correspond to the lowermost parts and a gradual upsection increase is observed for all the sections. However, the Na_2O has very low values (always < 0.54) hence the ratio generally fluctuates due to K_2O content (Appendix. 3). From bottom to top the K_2O/Na_2O increases from 5.67 to 89.6 in the Nammal Gorge (Fig. 2b), from 26.1 to 76 in the Gulla Khel while no significant change is observed in the Paniala section where the ratio fluctuates from 38 to 46.75. The highest K_2O/Na_2O values are recorded for the shales of the boundary bed at all the studied sections (Figs. 6b).

In the Datta Formation the K_2O/Na_2O range diminishes (0–44.3). The samples from the laterites, CBFA and sandstones-siltstone of the CMOFA display ratios generally below 10 whereas the shales of the CMOFA have relatively higher ratios (10 − 20). These can be easily differentiated from the shales of the LFA which possess the highest ratios (generally > 20).

4.5.3. A–CN–K plot

The A–CN–K ternary plot for the representative samples displays a cluster of samples near the A vertex close to the A–K side (Fig. 7a). Majority of the Triassic samples plot in the muscovite – illite position. The laterite/bauxite horizons of all the sections are clustered at A vertex corresponding to kaolinite position. The CBFA and associated sandstones-siltstones of CMOFA plot close to the A vertex above the Illite position. Most of the shales of the CMOFA and many of samples from the LFA plot in the illite – high illite zone. The CIA values are plotted for the samples to the left of the A–CN–K plot and correspond to the kaolinite – illite zone and are close to the A vertex of the diagram (Fig. 7a).

4.5.4. The chemical maturity plot (SiO_2 vs. $Al_2O_3 + Na_2O + K_2O$)

The quartz (SiO_2) vs. feldspars ($Al_2O_3 + Na_2O + K_2O$) plot roughly represents an isosceles triangle with SiO_2 line (y-axis) as its base and the two equal sides intersecting at 50% SiO_2 and roughly 30% $Al_2O_3 + Na_2O + K_2O$ (Fig. 7b). All the samples from the Kingirali Formation plot on the lower side of the diagram. The lowermost samples plot at the bottom side of the plot while, as we move upsection, the sample positions gradually move upward on the lower side of the triangle. The boundary beds from all the sections are clustered around the lower part of the vertex where the two equal sides meet (Fig. 7a).

The laterites/bauxites of the Datta Formation plot to the right of the vertex where the two equal sides meet and thus can be easily differentiated from the underlying boundary beds (Fig. 7b). The CBFA and CMOFA sands arrange close to the 100% SiO_2 vertex. The overlying CMOFA shales gradually move from the top vertex to where the two equal sides meet. Moving further upsection in the Datta Formation the shales and associated samples of the LFA plot close to the vertex where the two equal sides meet. However, these can be easily differentiated both from the shales of the Kingriali Formation and laterites of the Datta Formation as these occupy mostly the upper, equal side of the triangle (Fig. 7b).

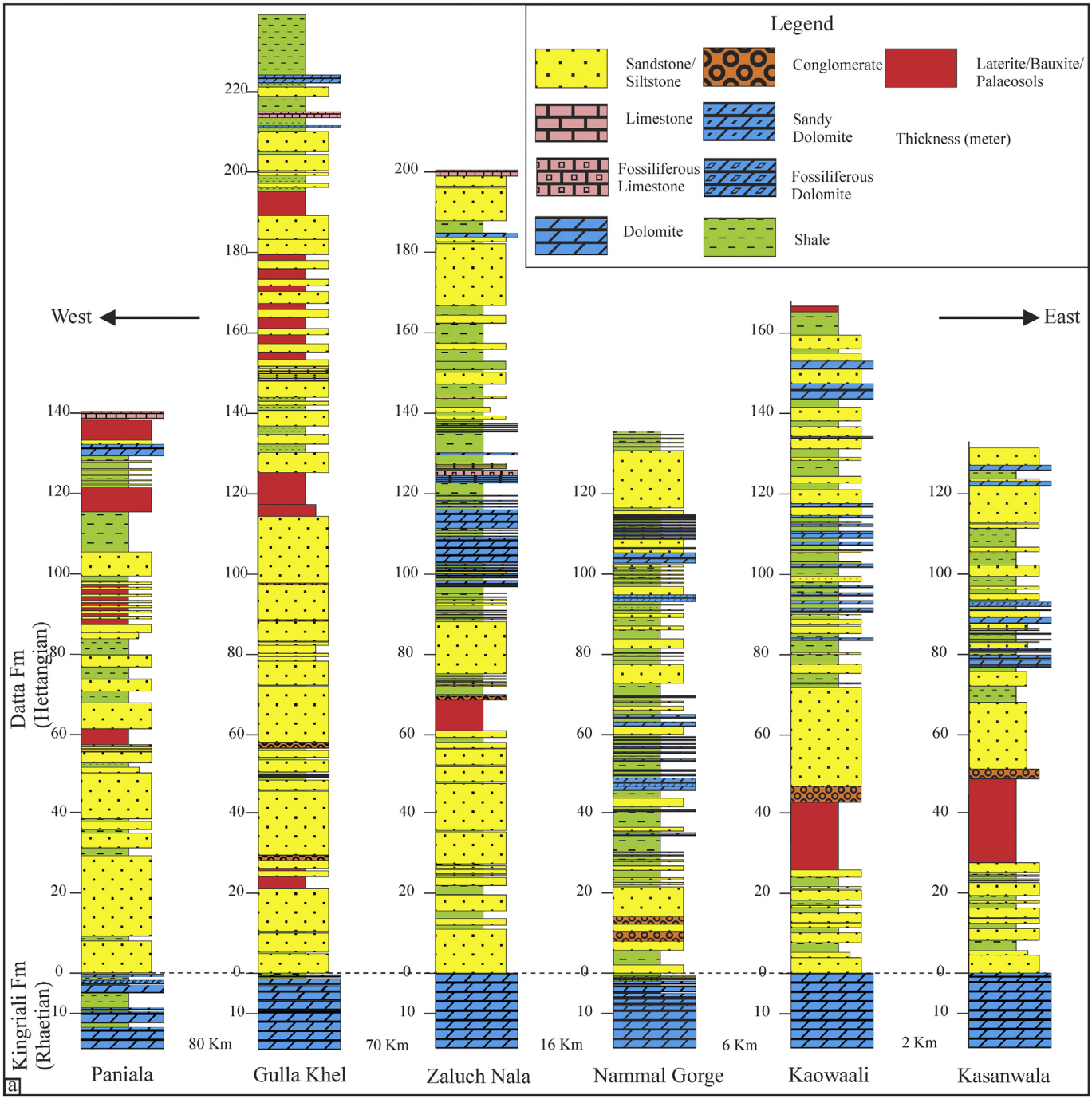

Fig. 2. (a) Representative measured stratigraphic sections in the Salt and Trans–Indus Ranges. The distance between each section is displayed in kilometres. (b) Representative section (Nammal Gorge) with various geochemical proxies plots highlighting the palaeoclimatic fluctuation in the section. CBFA = Channel Belt Facies Association, CMOFA = Channel Margin and Overbank Facies Association, LFA = Lagoonal Facies Association (see Fig. 2a for symbols and codes). The gray shaded area in the background indicates the Triassic–Jurassic transition.

5. Discussion

5.1. Outcrop/field sedimentology

The thick bedded, uniform and laterally persistent dolomites of the Kingriali Formation (Fig. 3a) represent platform carbonates deposited under an overall uniform palaeoclimate (Anwar et al., 1992). The shale/marls in the upper part of the formation, and their increase both in frequency and thickness (Fig. 3a) represents the establishment of a siliciclastic feeder system (and source) in the nearby area (Mount, 1984). These are also indicative of the gradual onset of climatic change with negative impact on carbonate production (Wood, 1990). The intraclasts bearing dolomite, with its flatly aligned pebbles (Fig. 3b), and the ferruginous dolomite (Fig. 3f) indicate a sea-level drop, reworking in very shallow water and at least part-time emergence. The overlying thin bedded gypsum and gypsiferous shale (Fig. 3f) represent the final demise of carbonate production. On the other hand, the gypsum also supports the establishment of hypersaline conditions and evaporites precipitation an evidence for warm and dry conditions (Tucker, 2009).

The quartz-rich conglomerates and associated quartz arenites in the lower part of the Datta Formation (Fig. 3a, c, e) indicate a prominent regression above the marine carbonates and the onset of coarse-grained

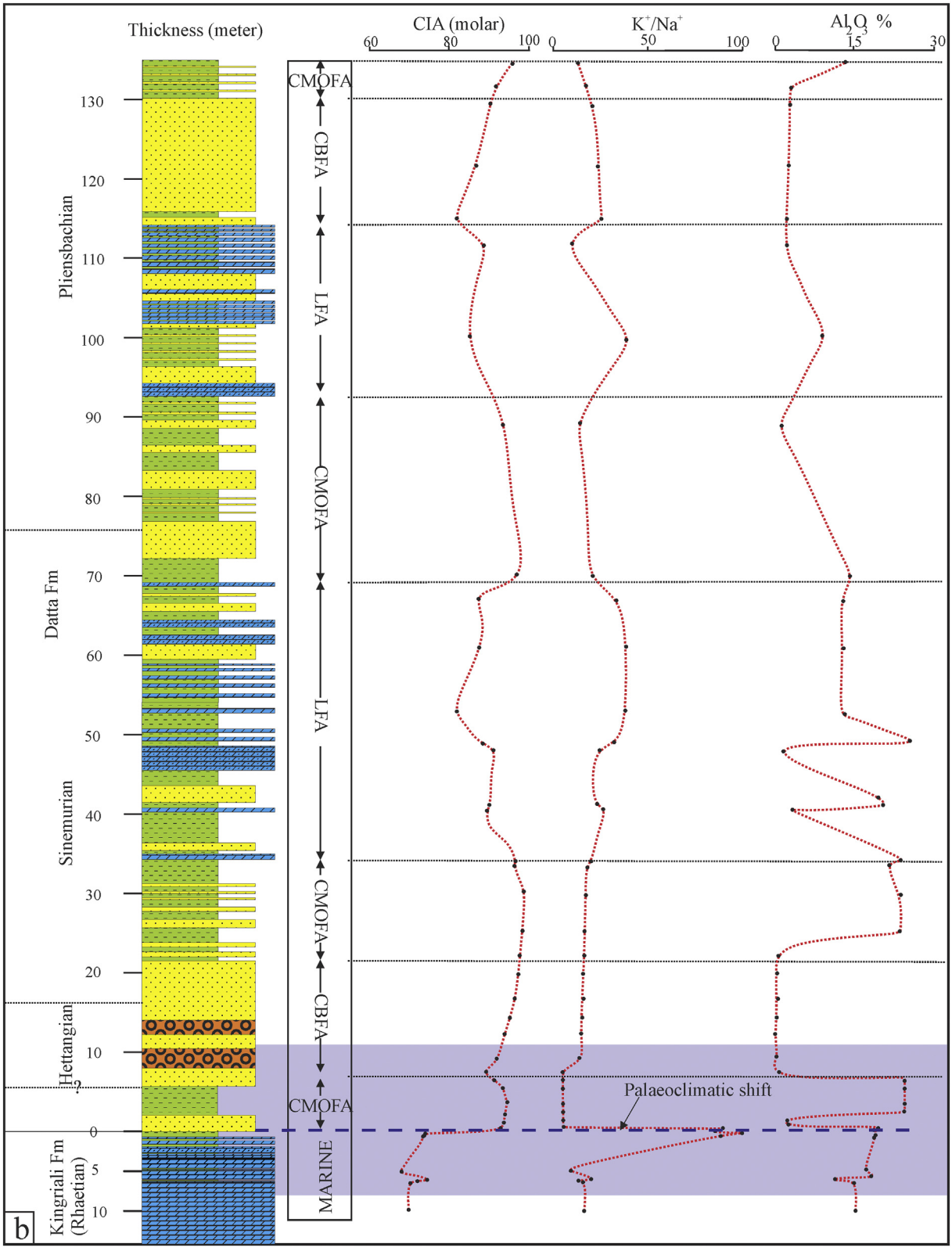

Fig. 2. (*continued*)

fluvial-continental conditions (Iqbal et al., 2015b). The occurrence of coal patches, plant remains and petrified wood (Fig. 3g) within the CBFA and the overlying CMOFA support a warm and humid palaeoclimate during their deposition. The associated laterites/bauxites and palaeosols (Fig. 3e) indicate hot and humid, waterlogged areas of a tropical to subtropical climate (e.g. Retallack, 2010; Mindszenty, 2016). Further upsection (Fig. 2a, b), the LFA represents transgression and onset of marine to marginal marine condition (Iqbal et al., 2015b).

5.2. Framework composition/petrography

The lower and middle part of the Kingriali Formation lacks

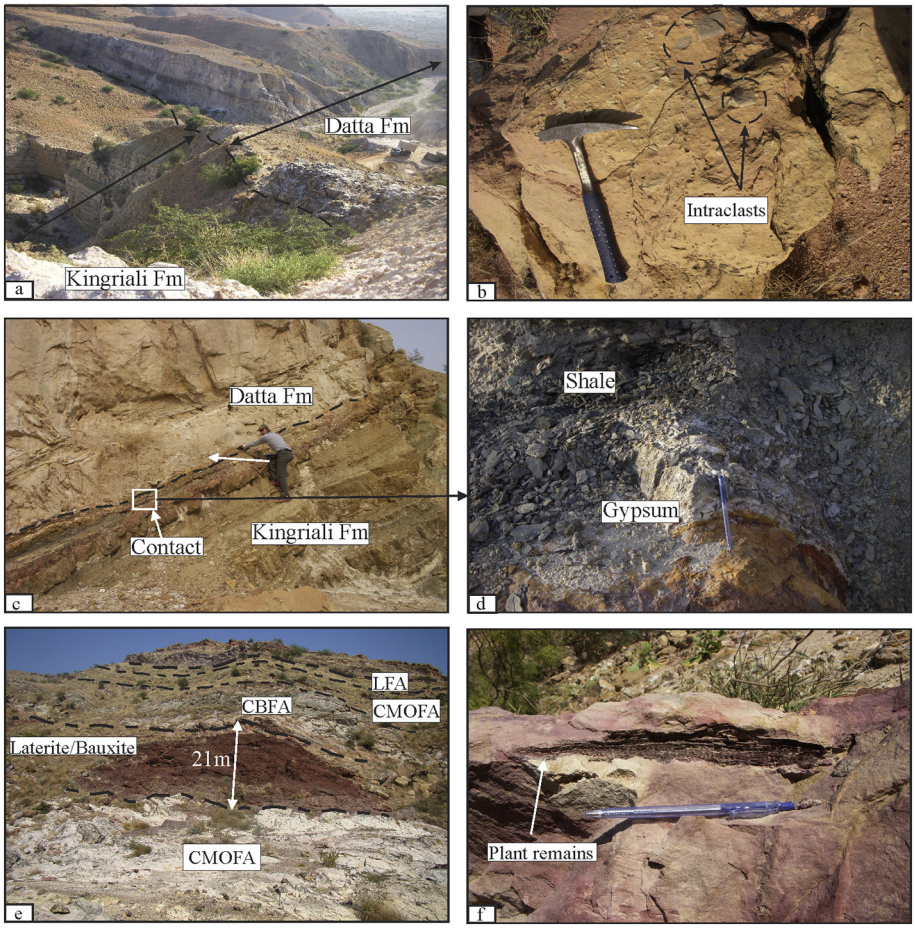

Fig. 3. Representative field photographs from the measured sections. (a) field view of the Kingriali and Datta formations at Paniala anticline section (Khisor Range). (b) intraclasts in the upper part of the Kingriali Formation at Kasanwala Section. (c) Triassic–Jurassic boundary in Paniala anticline section. (d) dark shale, gypsum and rusty brown dolomite in Paniala anticline section. (e) field view of the facies and facies associations in the Datta Formation at Kasanwala Section. (f) plant remains in the Datta Formation at Nammal Gorge. (Abbreviations are explained in the text and Fig. 2).

identifiable fauna; however, the uniform oolitic texture, micritic nature, occurrence of bivalves and gastropods (Fig. 4a, b) coupled with persistent sediments cycles reveals a depositional setting with only minor palaeoclimatic variations, probably subtidal depths on a large carbonate platform (Anwar et al., 1992). In contrast, the presence of intraclasts aligned parallel to bedding planes and reworked bioclasts (Fig. 3b) in the upper part of the formation advocate a significant drop in sea-level and/or accompanying tectonic activity (Sa'ad and Al-Mashaikie, 2017). Furthermore, the stromatolites (occurring in the overlying beds), normally flourish in the hypersaline and intertidal to supratidal conditions; on the other hand their occurrence supports the lack of dominant predators/grazing organisms and thus a possible biotic crises (e.g. Marzoli et al., 2004; Luo et al., 2016). Thus their occurrence may represent the transition to extreme conditions during the Triassic–Jurassic boundary interval (Jenkyns, 1988; Olsen, 1999; Pálfy and Smith, 2000). Also, the stromatolites generally occur in the shallow to very shallow water (Preto et al., 2015). In the present case, their stratigraphic position between the underlying shallow water, reworked, ferruginous carbonates and the overlying gypsum beds indicates near surface/at least partly emergent, intertidal to supratidal conditions. The Triassic strata thus present a similar situation as evidenced worldwide as a result of a significant and global eustatic sea-level drop at the Triassic–Jurassic boundary (Clemmensen et al., 1998; Hallam, 2001).

Quartz arenites constitute the major part of the Datta Formation (Fig. 2a, b) are texturally and compositionally supreme mature sandstones (Fig. 4c – e) and are the products of multi cyclic sediments transport and deposition (Pettijohn and Potter, 1987). Simultaneously, these are the product of intense and persistent chemical weathering, conditions that generally favour long, continued crustal stability (mostly at passive margins), warm/hot and humid palaeoclimates (Nichols, 2009; Dill, 2016). In the present case the dominance of quartz, absence or very minor occurrence of feldspars and complete absence of ferromagnesian minerals support deposition under such a hot and humid palaeoclimatic setting. Furthermore, Q_{mue} constitutes around 80% of the total quartz, suggesting very strong sorting. Such conditions are generally common in tropical and near tropical palaeoclimatic belts and also suggest a recycled origin of the sediments (Blatt, 1982).

The QFR triangular plot and the bivariant log/log plot of $Q_P/(F + R)$ vs. $Q_{total}/(F + R)$ indicate closely clustered sample populations in the humid part of the plot (Fig. 5a, b). These plots again support a humid palaeoclimate during the deposition of the Datta Formation. Primary absence of unstable minerals in the source areas may question the validity of the present interpretation. However, petrographic studies in the potential source areas reveal the presence of abundant feldspars and other, potentially unstable minerals (Ghazi and Mountney, 2011; Iqbal et al., 2015b; Jan et al., 2017).

5.3. Bulk mineralogy/XRD

The presence of only carbonates in the lower and middle parts of the Kingriali Formation (Appendix. 2) indicates carbonate precipitation without (silici)clastic interruption. Upsection the presence of both calcite and dolomite in the fossiliferous carbonate horizons may indicate selective dolomitisation where the bioclasts may have partly or completely survived dolomitisation, thereby preserving the original calcitic composition (Fig. 4a, b). Such an overall vertical distribution of dolomite on the platform does not reflect long-term eustasy (Balog et al., 1999). The thorough/intense dolomitisation of the lower platform part reflects a semiarid, hot subtropical, seasonal setting and mega-monsoonal climate. Global cooling and increased humidity toward the Latest Triassic inhibited pervasive early dolomitisation, leaving the

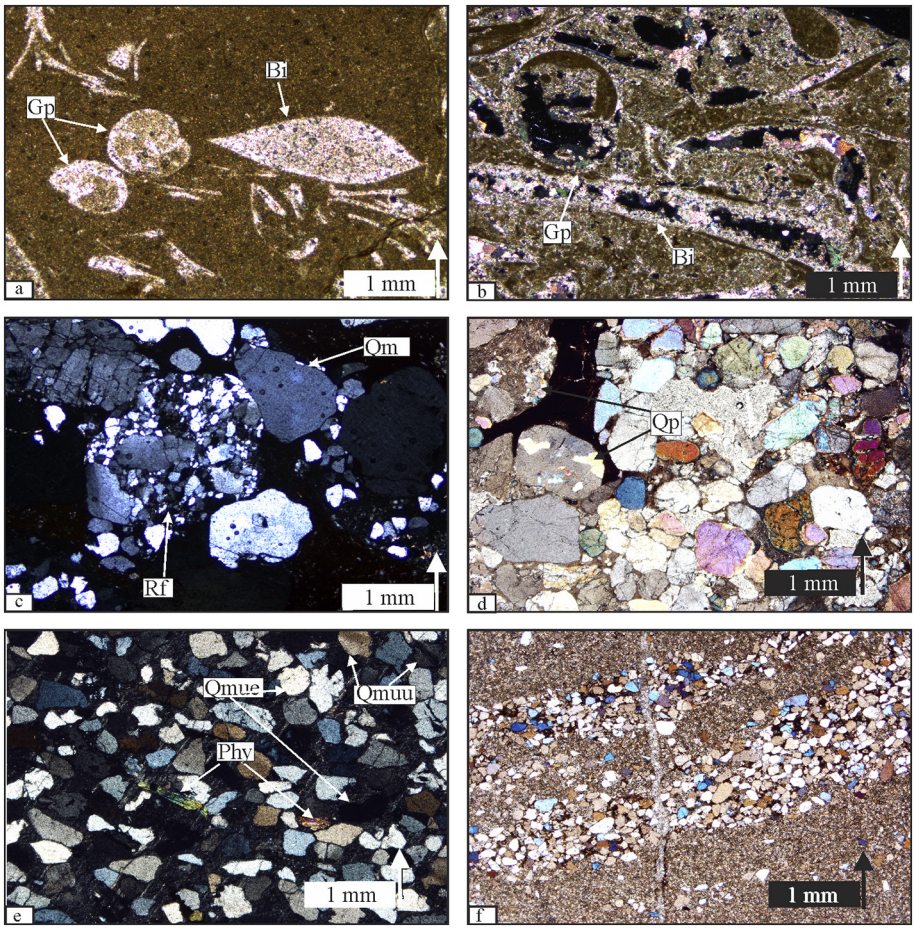

Fig. 4. Representative thin section photomicrographs from the measured sections. (a, b) bivalves (Bi) and gastropods (Gp) in the upper part of Kingriali Formation at Kasanwala Section. (c, d, e) rock fragments (Rf), monocrystalline quartz with unit extinction (Qmue), monocrystalline quartz with undulose extinction (Qmuu), polycrystalline quartz (Qp), phyllosilicates (phy) in the Datta Formation. (f) dolomite with quartz pulses in Kaowaali section.

upper platform largely as limestone (Balog et al., 1999). The gradual appearance of clay minerals and quartz indicates a gradual onset of the siliciclastic supply to the basin. The upsection disappearance of carbonates and increase in the clay contents indicates a demise of carbonate precipitation. The overlying evaporites (gypsum) also support semiarid to arid palaeoclimate and a probable drop in sea-level.

The CBFA of the Datta Formation, with dominant quartz peaks, supports the quartz-rich framework composition (Fig. 5a, b). At places, the very minor kaolinite peaks within these samples on one hand indicate the alteration of feldspars to clay minerals under greenhouse conditions (Dill, 2016). On the other hand, clay minerals introduction into the pore spaces during the comparatively low energy state of the flowing water could cause such deposition (Boggs Jr., 2009). However, the pore-space filling kaolinite is generally composed of concertina-type kaolinite and occurs in kaolin arkoses whereas in the active channel system kaolinite is accumulated mainly in the fine-grained overbank mudstone deposits (Dill, 2016). In the present case though, field and petrographic observations favour the overbank mudstones depositional scenario.

The overlying palaeosols, laterite/bauxite horizons are characteristically rich in kaolinite, boehmite and haematite. Such compositions rarely occur in warm semiarid – arid climates where surficial chemical weathering is only a minor process or is absent and also in cold and glacial climates where surficial chemical weathering proceeds very slowly and frost wedging is the dominant process (Tucker, 2009). Such deposits generally occur as residual deposits on passive continental margin and in epicontinental basins (Dill, 2016). The carbonates and shales of the LFA mark the onset of next marine/lagoonal settings (Iqbal et al., 2015b).

5.4. Clay mineralogy

The overall dominance of illite in the Triassic shales (Appendix. 2b) supports dry semiarid to arid conditions of deposition during Rhaetian (Keller et al., 1954; Singer, 1984; Han et al., 2014; Dill, 2016). The gradual upsection increase in the kaolinite content indicates a transition to warm-hot and humid palaeoclimate. The absence of kaolinite in the green shales (boundary bed) may be interpreted as representing arid and potentially cooler conditions established during volcanic winters (Schoene et al., 2010). The overlying shales of the Datta Formation are enriched in kaolinite (Fig. 7) and support hot, warm and humid palaeoclimate also indicated by other proxies.

A possible diagenetic control (Worden and Burley, 2003) over the clay minerals distribution may hinder their palaeoclimatic. Diagenetic history of kaolinite (Dill, 2016) is illustrated by a sequence of change from kaolinite through dickite into nacrite under increasing temperature and a conversion of halloysite into metahalloysite as the temperature decreases (Harvey and Murray, 1990; Polyak and Guven, 1996; Harrison and Greenberg, 1998). However, no such compositional variations were found in the present case. On the other hand it is also known that illite generally occurs in association with carbonates away from major rivers while kaolinite generally occurs in fluvial-alluvial settings (Weaver, 1958; Whitehouse et al., 1960; Thiry, 2000).

5.5. Bulk geochemistry

5.5.1. Chemical index of alteration (CIA)

CIA values mainly dependent upon chemical weathering and the latter has a direct relationship with the intensity of temperature and humidity of the prevailing (palaeo)climate (Nesbitt and Young, 1984). The relatively low CIA values for the Kingriali Formation (Figs. 2b, 7)

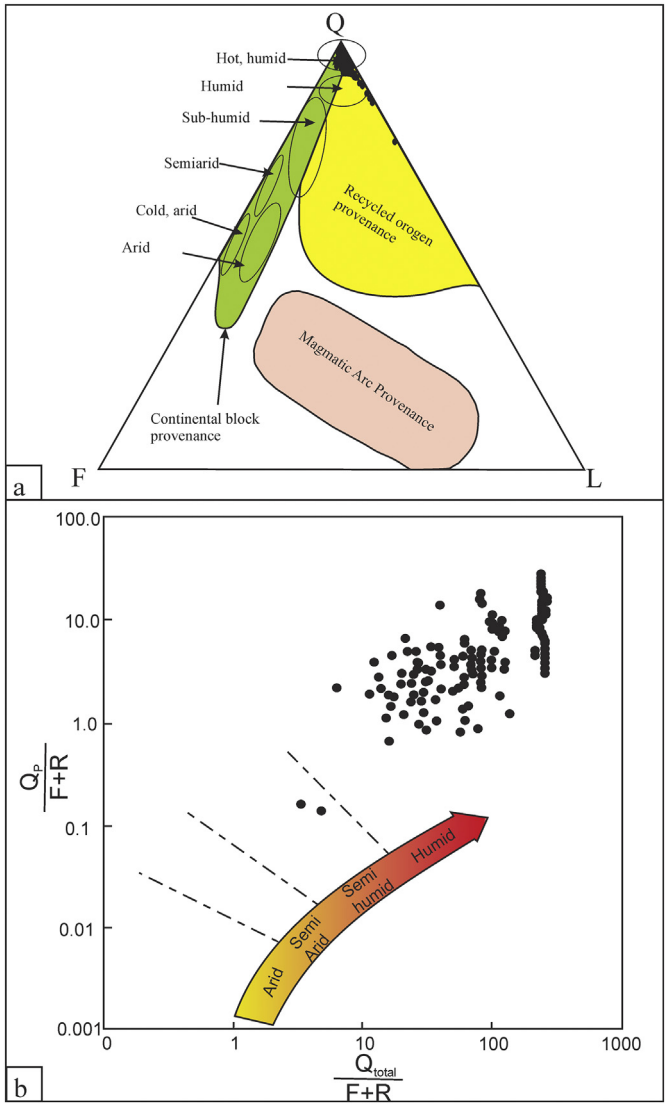

Fig. 5. (a) Quartz-Feldspar-Lithic fragments (QFL) plot for the representative samples of the Datta Formation. (b) log – log plot of polycrystalline quartz (Q_p)/(F + R) vs. total quartz Q_{total}/(F + R).

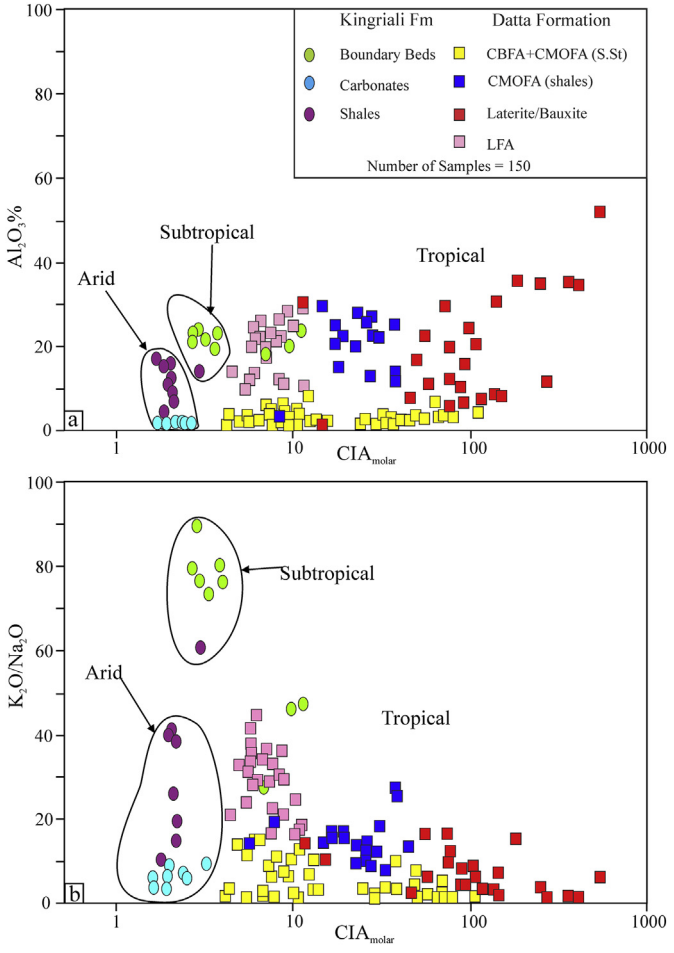

Fig. 6. (a) Al_2O_3 vs. Chemical Index of Alteration (CIA_{molar}) plot for the representative samples. (b) K_2O/Na_2O vs. CIA_{molar} plot for representative samples.

indicate a lowered intensity of chemical weathering during the Late Triassic and hence deposition under semiarid to arid palaeoclimate. However, the gradual upsection increase in the CIA values supports a gradual onset of increasing humidity in a warming, subtropical to tropical palaeogeographic setting (Figs. 6a, b). The highest CIA values correspond to the topmost beds in every section indicating the onset of comparatively warm-hot and humid palaeoclimate during the Triassic–Jurassic transition.

The high CIA values for the CBFA and CMOFA suggest their deposition in hot and humid palaeoclimate (Fig. 2b). The palaeosols of the CMOFA and the laterite/bauxite horizons possess the highest CIA values (all above 95), thus confirming their deposition under extreme greenhouse condition in tropical – near tropical palaeoclimates (Mindszenty, 2016). Further upsection, the gradual drop in the CIA values (Fig. 2b) in the LFA indicates the onset of lagoonal/marine conditions with siliciclastic input under prevailing warm and humid conditions. The second depositional sequence displays warm - humid tropical palaeoclimate.

5.5.2. Al_2O_3 vs. CIA and K_2O/Na_2O vs. CIA Plots

Scatter plots of Al_2O_3 vs. CIA and K_2O/Na_2O vs. CIA, calibrated with modern examples from different climates, have been used in literature to interpret climate conditions (e.g. Goldberg and Humayun, 2010 and references therein). The initial siliclastic influx in the upper part of the Kingriali Formation, marked by a vertical increase in the Al_2O_3 content (up to 15%) and no visible increase in the CIA value, indicates the onset of fine grained siliclastics under comparatively stable palaeoclimate (Figs. 2b, 6a). The overall low Al_2O_3 content of this zone also support semiarid to arid conditions globally reconstructed for the Late Triassic (Frakes, 1979; Allen et al., 1994; Balog et al., 1999; Ruckwied and Götz, 2009; Luo et al., 2016). The gradual upsection increase in both the Al_2O_3 and CIA (Fig. 6a) indicates a transition to a comparatively humid setting. The topmost samples (boundary beds) plot in the subtropical palaeoclimate. However, the associated evaporites are indicative of high evaporation under arid conditions.

The Lower Jurassic samples plot in the tropical settings (Fig. 6a). The CBFA and CMOFA display higher CIA values but the Al_2O_3 content is understandably lower than 10% as these are quartz arenites (Fig. 2b). The shales and palaeosols of the CMOFA have high CIA and Al_2O_3. The highest CIA and Al_2O_3 occur in laterite/bauxite samples. The high kaolinite content within these horizons presents a strong case of hot and humid palaeoclimate and thus greenhouse conditions. The relatively medium kaolinite content of the shales of the LFA also explains the relatively medium Al_2O_3 values (15–25%) and comparatively low CIA values (Fig. 6a). The second cycle of the Datta Formation in the study area displays a similar trend.

The K_2O/Na_2O vs. CIA provides refined interpretation of the palaeoclimate as the K_2O content is a function of the illite content within

the samples (Song et al., 2014). In the present case the K_2O/Na_2O vs. CIA plot for the Kingriali Formation shows a population cluster in the arid setting (Fig. 6b). However, an increasing upsection trend in the K_2O/Na_2O ratios supports a gradual transition from arid – semiarid to humid palaeoclimate. The widest K_2O/Na_2O range (5.6–89.6) in the Nammal Gorge (Fig. 2b) reflects the selective removal of Na^+ content, while K^+ (and hence illite) is highest and thus indicates weak chemical weathering in an arid setting. Westward, the decrease in K_2O/Na_2O range and so too in both the Na^+ and K^+ reveals transformation of illite to kaolinite (Song et al., 2014). The boundary beds display subtropical palaeoclimate weathering trends (Fig. 6b).

The small K_2O/Na_2O range (0–44.3) for the Datta Formation coupled with high CIA values supports overall tropical conditions (Fig. 6b). The CBFA and sandstones-siltstones of the CMOFA, with ratios generally below 10, suggest the removal of K^+ and Na^+ (both K-feldspar and plagioclase) under warm humid conditions. The overlying palaeosols and laterites/bauxites also display K_2O/Na_2O ratios below 10 and their kaolinite dominance supports tropical water-logged settings (Dill, 2016). The relatively high K_2O/Na_2O ratios (10–20) of the overlying shales of the CMOFA make their differentiation from the LFA easier as the latter possess the highest K_2O/Na_2O ratios (generally > 20) within the Datta Formation. The second depositional cycle displays a warm-humid palaeoclimate.

5.6. A-CN-K plot

The A–CN–K ternary plot (Fig. 7a) indicates weathering trends (Selvaraj et al., 2004; Selvaraj and Chen, 2006). In the present case, the linear cluster of samples between A vertex and muscovite position along the A-K side favours a recycled origin of the sediments. Most of the Rhaetian samples plot in the muscovite – illite position thereby favouring semiarid to arid conditions. The lowermost samples in the entire sections plot in the muscovite position. As we go upsection, the progressive upward plot of the samples close to the illite zone indicates a gradual increase in the intensity of the chemical weathering.

The cluster of samples from the palaeosols, laterite/bauxite horizons, sandstones and siltstones of CBFA and CMOFA plot correspond to the kaolinite position. An east to west increasing chemical maturity trend is indicated by shales of the CMOFA and the LFA plot in the illite – kaolinite zone. In this trend, the Nammal Gorge and Zaluch Nala samples occupy positions in the illite – high illite – kaolinite zone while most of the samples from the Gulla Khel and Paniala section plot in the kaolinite zone, a strong support of recycling under a hot/warm and humid palaeoclimate. The CIA correlation with the A–CN–K plot (Bahlburg and Dobrzinski, 2011) shows a strong coherence between the two data sets (Fig. 7a).

5.7. The chemical maturity Proxy Plot (SiO_2 vs. $Al_2O_3 + Na_2O + K_2O$)

Good correlation between the increasing SiO_2 content and $Al_2O_3 + Na_2O + K_2O$ for the Kingirali Formation (Fig. 7b) indicates gradually increasing siliciclastic influx that eventually inhabited carbonate precipitation upsection. This trend also supports increasing upsetion chemical maturity. The lower samples plot in arid zone, the upper correspond to the semiarid part and the boundary beds plot between semiarid and semi-humid zones. Thus the Upper Triassic samples mark a gradual change from arid palaeoclimate to a semiarid – semi humid palaeoclimate (Fig. 7b).

The palaeosols, laterite/bauxite samples of the Datta Formation plot in the semi-humid to humid zone (Fig. 7b) indicating the onset of humid condition during the earliest Jurassic following the Rhaetian aridity. It is important to mention here that the laterite/bauxite samples, that are highly enriched in Al_2O_3 (kaolinite) content, plot with this method erroneously in the arid – semiarid part of the plot. These should not be mistakenly interpreted as the product of dry palaeoclimate, as these have lost their SiO_2 due to dissolution under extreme greenhouse conditions and thus inevitably are a product of very high intensity of chemical weathering.

The sandstones to siltstones of the CBFA and CMOFA plot close to the 100% SiO_2, thus they represent deposition under very high humidity and warm/hot temperatures, interpreted in previous sections (Figs. 5a, b). The shales of the CMOFA and LFA are positioned in the humid part of the plot favouring their deposition in hot, warm and humid palaeoclimate (Fig. 7b).

6. Interpretation of results

6.1. Prevailing palaeoclimate

Following the deposition of the lower and middle parts of the platform carbonates of the Kingriali Formation, a siliciclastic system gradually started during the Rhaetian in the Salt and Trans–Indus Ranges (Fig. 8). This siliciclastic supply gradually increased until the carbonate production completely gave way to a siliciclastic-rich system at the Triassic–Jurassic boundary. Following this initial phase, the siliciclastic system established depositing the fluvio-deltaic Datta Formation (Iqbal et al., 2015b).

Field evidences, framework mineralogy, XRD, clay mineralogy and bulk geochemistry of the Kingriali Formation indicate a semiarid to arid palaeoclimate in the source area and the depositional basin during the Rhaetian. Such conditions are generally common in warm-semiarid to arid and also in glacial regions (e.g. Singer, 1984; Boggs, 2006). In the present case glacial evidence do not occur in the area (Iqbal et al., 2015b), nor does the subtropical – near tropical palaeogeographic position of the area during this time interval (Fig. 1a) support any possibility of glaciation. Furthermore, globally there are no evidences for glaciation in the Late Triassic (Meyen, 1997; Sellwood and Valdes, 2006).

The uppermost part of the formation with increasing kaolinite content, increasing upsection trend in CIA reveals a gradual onset of the chemical sorting toward the top of the Kingriali Formation. This indicates the onset of a climate transition toward more humid conditions during the Triassic–Jurassic boundary interval (Fig. 8). Samples from the boundary beds have higher illite content that would indicate cool and dry climate. However, the gypsum beds within the boundary interval (Fig. 3d) also support evaporation in a warm and arid palaeoclimate.

The used proxies for the Datta Formation unequivocally indicate hot/warm and humid palaeoclimate during Early Jurassic (Fig. 8). The framework composition plots indicate quartz arenites of the high humid zone (Fig. 5a, b). XRD analysis proofs the presence of only quartz within these samples. The kaolinite, boehmite and haematite-rich mineralogy of the palaeosols and laterite/bauxite horizons indicates long, continued intense chemical weathering under greenhouse conditions. The CIA displays the highest values (> 90) for these zones within the formation confirming the hot – humid tropical near tropical palaeoclimate (Figs. 2b, 6). The Al_2O_3 vs. CIA plot of these intervals indicate extreme tropical climate that is also confirmed by the K_2O/Na_2O vs. CIA plot (Fig. 6a, b). The A–CN–K plot shows a cluster of these samples in the kaolinite zone (Fig. 7a) again confirming their supreme mature stage of chemical alteration. The SiO_2 vs. $Al_2O_3 + Na_2O + K_2O$ plot for these horizons show humid conditions (Fig. 7b). The kaolinite rich mineralogy of the shales of the CMOFA and LFA shows (Appendix. 2) deposition under hot/warm palaeotemperatures and high humidity.

6.2. Lateral variations

The multi-proxy palaeoweathering data provide information about east-to-west lateral variations and gradients. The shale to dolomite ratio in the upper part of the Kingriali Formation decreases from east (2.6 at Nammal Gorge) to west (1.5 at Paniala). This, on one hand indicates the proximity of the eastern part to the siliciclastic feeder source area; on

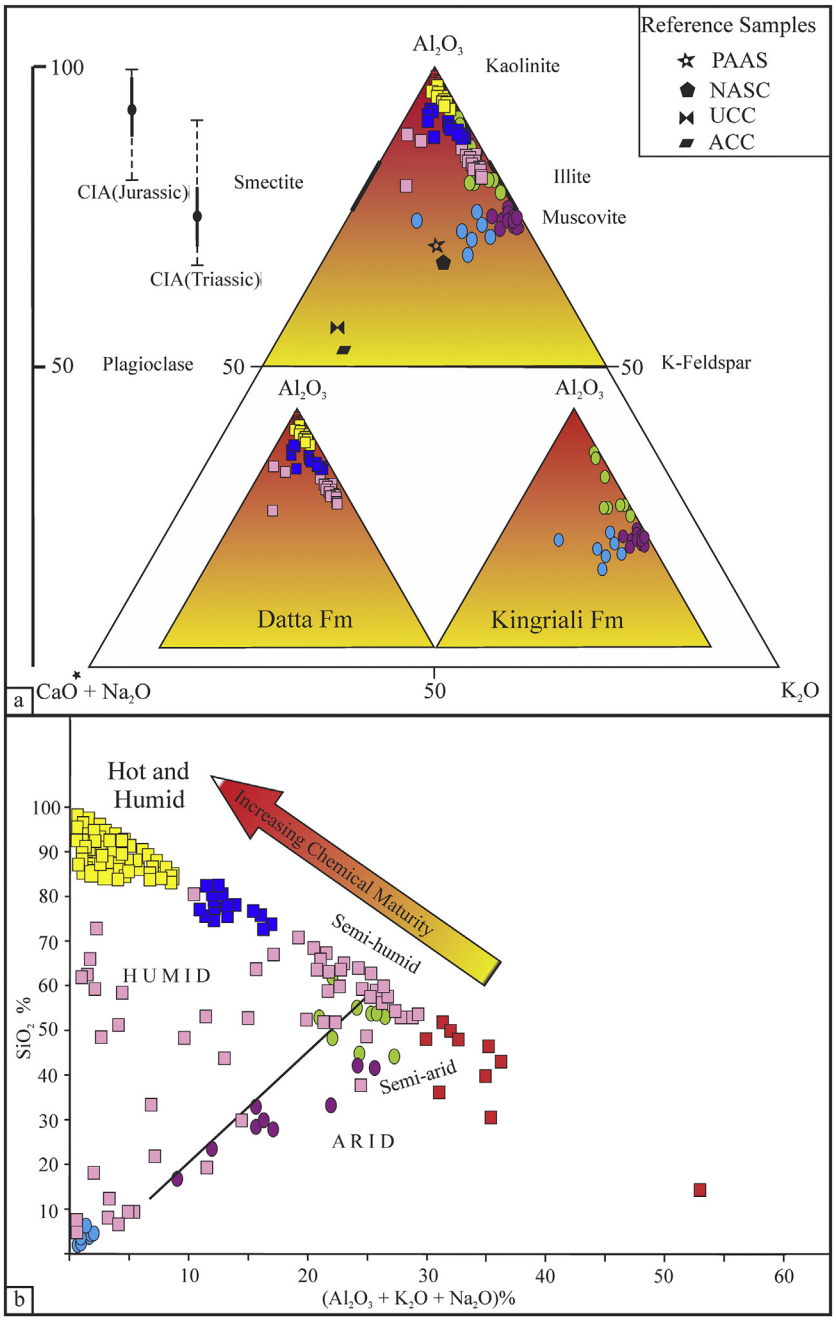

Fig. 7. (a) A–CN–K plot for the representative samples, positions of reference minerals (muscovite, illite, smectite and kaolinite) are indicated on the plot (Basu, 1976; Nesbitt et al., 1996). The Triassic and Jurassic samples are separated in the lower part of the plot and the CIA range (dotted and dashed lines) and average (black dots) is plotted to left for both the Triassic and Jurassic samples. The reference samples include Post Archaean Australian Shale (PAAS), North American Shale Composite (NASC), Upper Continental Crust (UCC) and Average Continental Crust (ACC) (Gromet et al., 1984; Nesbitt et al., 1996; Rudnick and Gao, 2003). (b) Compositional maturity proxy plot for SiO_2% vs. $(Al_2O_3 + K_2O + Na_2O)$% showing palaeoclimatic conditions during the deposition.

the other hand it supports the lack of an efficient transport mechanism for the sliciclastics during Late Triassic. The thin bedded gypsum and gypsiferous shale present at the contact with the Datta Formation in Nammal Gorge, Gulla Khel and Paniala anticline sections support the uniform semiarid – arid conditions suitable for evaporites precipitation. CIA values for the Kingriali Formation indicate low intensity of chemical weathering and a general east-to-west increase (Kasanwala and Nammal Gorge sections: 73.6, to Paniala anticline section Khisor Range: 82.9). The A–CN–K plot, K_2O/ Na_2O ratios and other proxies confirm this east-to-west increase in the chemical maturity.

The Datta Formation has overall mature sediments, a product of clearly more hot and humid palaeoclimate under partly extreme greenhouse tropical to subtropical conditions. Quartz-rich conglomerates are dominant in the western Salt Range and are absent in the Trans–Indus Ranges corroborating an east-to-west clastic sediment transport. The overall geochemical analyses do not display any major east-to-west geochemical variation.

7. Possible drivers of palaeoclimate variations

7.1. Palaeogeography

The Triassic, a hothouse time with ice free poles (Preto et al., 2010), had a dominantly warm semiarid to arid palaeoclimate with an intervening Carnian humid episode (Ruffell et al., 2016). All the continents were locked into the supercontinent Pangaea, surrounded by the Panthalassa Ocean (Ziegler et al., 1983). The Tethys Ocean cut into Pangaea and was largely confined to the tropical to subtropical belt (Ziegler et al., 2003). These were the probable reasons for hot summers, relatively cold winters and strong monsoonal circulation in the circum-Tethyan part of Pangaea (e.g. Kutzbach and Gallimore, 1989; Dubiel et al., 1991; Jacobs and Sahagian, 1993). This mega-monsoon seasonality produced dry equatorial regions in the eastern part of Pangaea, facing the western Tethys (Parrish, 1993; Wang, 2009).

The palaeogeographic position of the study area on the

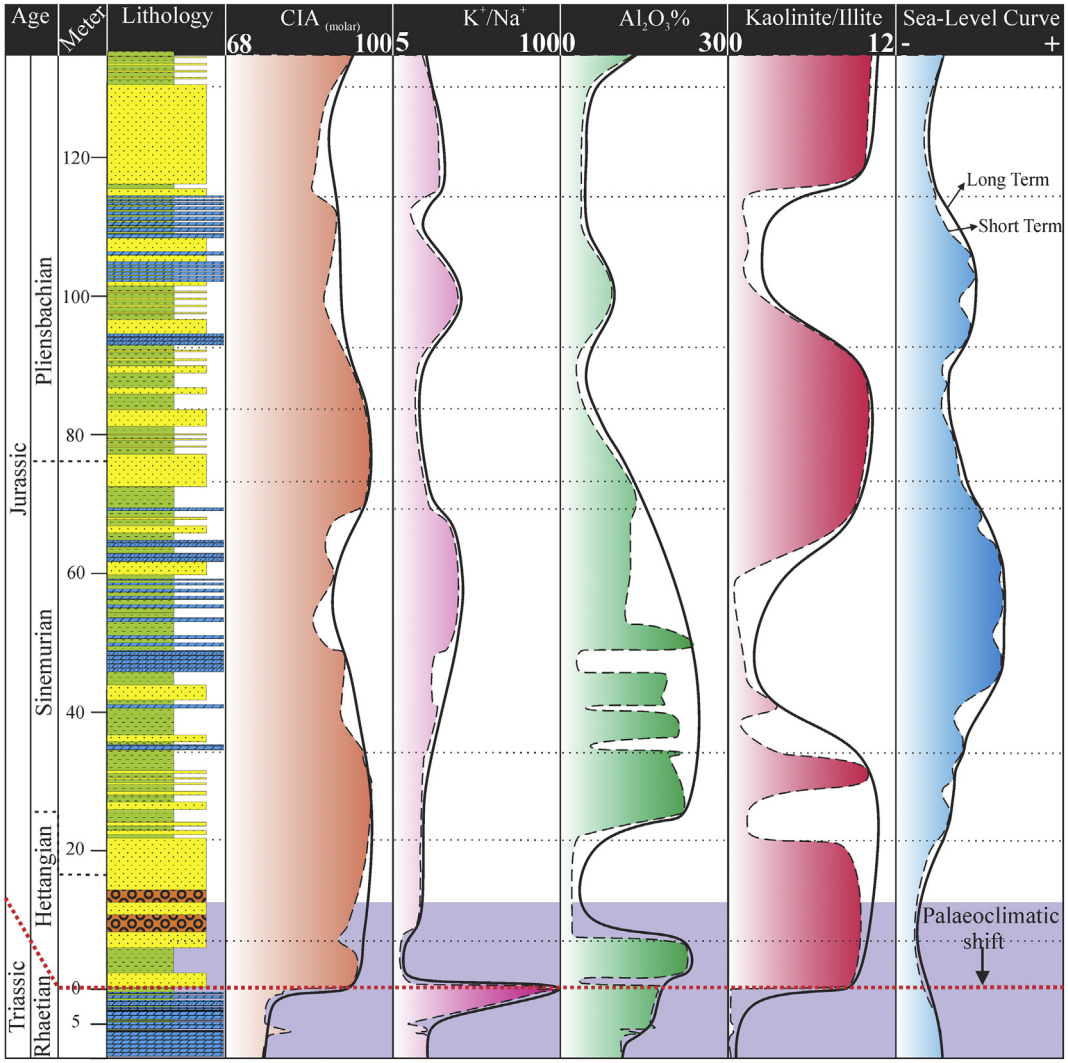

Fig. 8. Weathering and palaeoclimate trends across the Triassic–Jurassic transition, reconstructed from various proxies (CIA, K^+/Na^+, Al_2O_3, kaolinite/illite) together with sea-level fluctuations for the representative Nammal Gorge section (Salt Range). Note: the dashed lines in the proxies plots are the actual values calculated from the bulk geochemistry data for the CIA, K^+/Na^+ and Al_2O_3. The kaolinite/illite is calculated from the clay mineralogical composition for each sample. The minimum to maximum values ranges are given at the top of each curve. The solid lines represent the general trend derived from the actual values in each case. The increasing intensity of colour shades to the right indicates increasing values to the right side. The gray shaded area in the background indicates the Triassic–Jurassic transition. The dashed line in the sea-level curve indicates the short term trend and the solid line represents the long term trend during the Triassic–Jurassic transition. The Sea-level curve (not to the scale) is adopted from many resources (e.g. Haq et al., 1987; Hallam, 2001; Haq, 2017) and is corrected for the study area based on Iqbal et al., (2015b), detailed field and subsurface observations.

southeastern, equatorial – near tropical margin of Pangaea, facing the western margin of the Tethys (Fig. 1a), and the combined geochemical results affirm a warm, semiarid to arid palaeoclimate during the Rhaetian. However, in eastern North America, a narrow equatorial humid zone and an arid belt south of 30^O N, passing northward into humid temperate climates existed (Smoot and Olsen, 1988; Olsen and Kent, 1996, 2000; Kent and Olsen, 2000; Whiteside et al., 2011). The palaeogeographic position of the study area may be an example of the existence of such zonal climate north of 30^O in the southern hemisphere passing southward into humid climate. However, no significant shift in palaeolatitudes have been reconstructed for the study site from Late Triassic to Early Jurassic times (e.g. Schettino and Turco, 2011), so the climate evolution cannot be explained by plate movements through latitudinal climate zones.

7.2. Tectonics and CAMP volcanism activity

The latest Triassic stability in climates was followed by the end-Triassic mass extinction (ETE) event (Raup and Sepkoski Jr., 1982). This global catastrophic biotic turnover at 201.56 Ma (Blackburn et al., 2013) implies a dramatic climate turnover that coincides with the CAMP activity (Marzoli et al., 1999; Beerling and Berner, 2002; Marzoli et al., 2004; Davies et al., 2016). The CAMP activity (an area of $> 2.5 \times 10^6\ km^2$) forced a severe climate change via volcanic gases emissions. Recent studies reveal a warming trend from greenhouse to hothouse climate as an extinction mechanism (McElwain et al., 2007). Stomatal index data suggests increase of atmospheric CO_2 to around 2000–2400 ppm, in the boundary interval suggesting a 3^O – 4 °C warming (McElwain et al., 1999), whereas stable isotopic evidence suggests atmospheric CO_2 up to 4400 ppm (Schaller et al., 2011). Geochemical analysis of the European and Pacific basins indicates a substantial negative isotope anomaly (up to −3.5‰ $\delta^{13}C$) across the Triassic–Jurassic boundary at the ETE (Galli et al., 2005; Kuerschner et al., 2007; Ruhl et al., 2009; Greene et al., 2012; Bachan et al., 2014). This carbon cycle perturbation involved the massive release of greenhouse gases, i.e. ~8000–9000 Gt C as CO_2 during the CAMP basaltic

eruptions and ~5000 Gt C as CH_4 (e.g. Pálfy et al., 2001; Beerling and Berner, 2002). The CAMP activity is considered as the major reason for transition from dominantly warm, semiarid - arid to hot and humid greenhouse conditions (Korte et al., 2009; Kidder and Worsley, 2010).

In the study area there are no direct evidences of regional basaltic flow and volcanic ash layers have not been identified so far. However, the Karapa greenschist, 200 km to the north of the study area, extends from Westphalian to Carnian (Pogue et al., 1992). Further to the north/northeast, the Late Triassic Landai Formation (Allai Kohistan) and the Triassic–Lower Jurassic Alpurai Group of Swat–Bunair area have numerous amphibolitised basaltic horizons (DiPietro, 1990; Pogue et al., 1992; DiPietro et al., 1999). Unfortunately lack of reliable age control restrains any direct palaeoclimatic correlation between these basaltic layers and Salt and Trans–Indus Ranges.

Seismic reflection data reveal the presence of many subsurface, north-dipping basement normal faults in the Salt and Trans–Indus Ranges and Kohat–Potwar Plateau, terminating at the base of the Jurassic strata (Iqbal et al., 2015a). Furthermore, the Sargodha High, 50 km the south of the Salt Range, is considered as a horst structure uplifted during the Triassic–Jurassic boundary interval (Kadri, 1995). Most recently, this high has been considered not to be a part of the foreland normal-sense high strain zones that were active in the Paleoproterozoic (Martin, 2017), thereby supporting the younger age of Sargodha High. The nature and the timing of these faults provide strong evidences for the splitting and breakup of Pangaea in the Gondwanan domain comparable to CAMP activity (Iqbal and Wagreich, 2016). On the other hand, based on the palaeogeographic position of the study area to the nearby Karoo Rift, these tectonic features may be related to the initial phase of the Karoo Rift before the onset of main basaltic flow during Toarcian (Iqbal and Wagreich, 2016).

8. Regional and global correlation

The existing global correlation attempts on the Triassic–Jurassic transition are mostly focused on the Carbon Isotopic Excursion (CIE) emphasising the initial negative CIE (e.g. Hillebrandt et al., 2013; Lindström et al., 2017; Fig. 9). Unfortunately there is not much literature available on the Triassic–Jurassic boundary interval outside the European basins and North America (Laurasia). This study is the first detailed attempt from the then southern hemisphere (Gondwanaland) that explains the very close correlation with the Laurasia sections. An attempt has been made to correlate the geochemical spikes observed in the present studies to the Initial Negative Isotopic Excursion (InCIE) at famous localities in the New York Canyon, England and Northern Calcareous Alps (NCA) Austria (Fig. 9). However, since the study deals with the bulk geochemistry and clay mineralogy so detail discussion in this context in proved below:

Following the Carnian Pluvial Event, prolonged palaeoclimatic stability established in most parts of the European basins (Preto et al., 2010). Monotonous dolomitised peritidal carbonates successions (Dolomia Principale and Hauptdolomit) were deposited in the Alps under a hot and semi-arid climate (e.g., Haas and Demény, 2002) in a large carbonate platform setting (e.g. Frisia and Wenk, 1993; Iannace and Frisia, 1994; Meister et al., 2013). In northern Italy, the Travenanzes Formation (Preto et al., 2015) indicates deposition in a wide low-relief coastal area, dry land river – muddy coastal plain and sabkha system (Breda and Preto, 2011). Seaward of this clay-rich environment, thick peritidal carbonates formed in a large-scale epicontinental platform. In the Salt and Trans–Indus Ranges the Tredian Formation and the Chak Jabbi Limestone provide a similar facies and succession. The Tredian Formation is considered to have been deposited in a fluvial- deltaic setting (Iqbal et al., 2014). The Lower and middle parts of the Kingriali Formation can be considered as the stratigraphic equivalent of the Dolomia Principale and Hauptdolomit.

The Fleming Fjord Formation of east Greenland indicates deposition in semiarid–arid palaeoclimate with a change to a marginal warm moist temperate climate at the end of Rhaetian (Clemmensen et al., 1998). In southern Sweden, a transition from smectite dominated clays of the Maglarp B unit and the Kågeröd Formation (Norian and older) to smectite-free kaolinitic clays of the Höganäs Formation (Rhaetian – Hettangian) indicates a transition from arid to warm and humid conditions (Ahlberg et al., 2003).

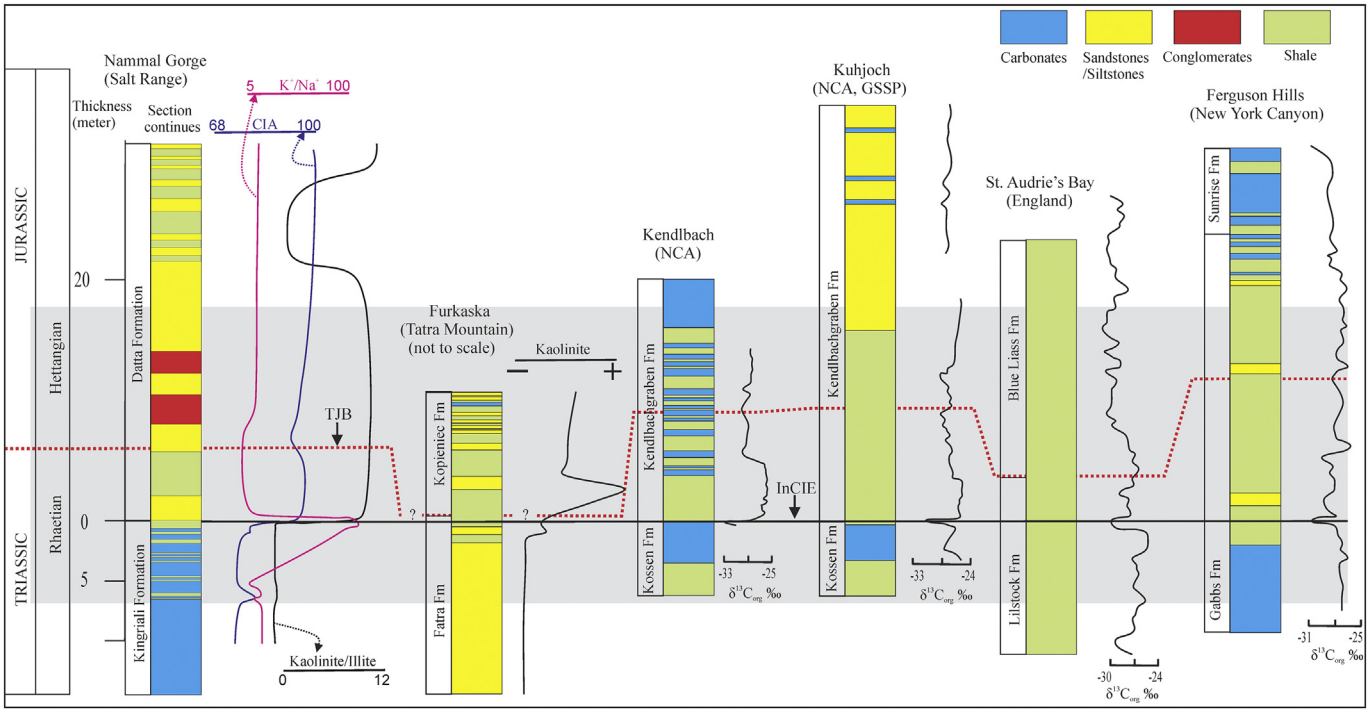

Fig. 9. A general global correlation of the geochemical results (Nammal Gorge) with the base-Jurassic Global Stratotype Sections and Point (GSSP) at Kuhjoch (Austria) and other famous sections (modified from Michalik et al., 2010; Pálfy and Zajzon, 2012; Hillebrandt et al., 2013; Lindström et al., 2017). With the exception of Furkaska (Tatra Mountain) all the other sections are on the same thickness scale.

In the Tatra Mountains, Slovakia, illite-smectite rich clays of the Carpathian Keuper and the Rhaetian Fatra Formation indicate arid environment (Michalik et al., 2013). Kaolinite appearance in the uppermost part of the Fatra Formation (~2%), reaching to a peak abundance of 11% in the Kopienec Formation (Hettangian) indicates the gradual onset of greenhouse conditions at the Triassic–Jurassic boundary (Michalik et al., 2010).

At Kendlbachgraben, Austria, geochemistry and clay mineralogy of the Rhaetian Eiberg Member of the Kössen Formation, and the overlying boundary mudstone "Grenzmergel" of the Tiefengraben Member of Kendlbach Formation support similar interpretation to southern Sweden (Bachan et al., 2014). The mineralogical and palynological studies of the Kendlbach Formation indicate a marked shift to humid climate and freshwater runoff (Bonis et al., 2010). Furthermore, geochemistry of the lowermost "Grenzmergel" have a distinctive enrichment in the heavy REEs (Pálfy and Zajzon, 2012). High kaolinite contents are reported from the topmost Triassic *Triletes* beds in Germany (Van de Schootbrugge et al., 2009).

The change in clay mineralogy in the studied sections provides a comparable palaeoclimatic transition from hot–semiarid–arid to a hot and humid setting. Geochemistry of the Triassic–Jurassic boundary interval (green shale) reveals abnormally high concentration of the total rare earths elements (REEs) comparable to that observed in the Newark Basin, Culpeper basin, Morocco (Marzoli et al., 2011) and in Kendlbachgraben section, Austria (Pálfy and Zajzon, 2012).

In Pomerania, Poland, the lower–middle Rhaetian siliciclastics (Wielichowo Beds) were deposited under semiarid palaeoclimate, whereas the Upper Rhaetian–Lower Hettangian Zagaje Formation (siliciclastics) was deposited in a fluvial-lacustrine environment under a humid period (Pieńkowski et al., 2012), similar to the change to a fluvio-deltaic to lacustrine/lagoonal setting in Pakistan.

9. Conclusions

In the Salt and Trans–Indus Ranges of Pakistan the thick, monotonous and laterally widespread lower and middle part of the Upper Triassic Kingriali Formation represents deposition of platform carbonates under stable warm, semiarid – arid palaeoclimate. During the latest Rhaetian, fine grained siliciclastic input of illite rich shales indicates a gradual onset of a siliciclastic system under semiarid – arid settings toward the Triassic–Jurassic boundary. The mineralogy and geochemistry of the topmost clay beds provides the possible links to Pangaea splitting and CAMP activity. The overlying kaolinite rich clay beds of basal part of the Lower Jurassic Datta Formation support high input of continental detritus and deposition under conditions of extreme chemical weathering. The quartz arenite nature of the coarse silicilastics, highly mature geochemistry, presence of coal beds – coal patches and abundant plant remains strengthen the prevalence of hot and humid greenhouse palaeoclimatic conditions during the deposition of the Datta Formation. The succession provides ideal sections from the then southern hemisphere for palaeoclimatic correlation with the northern hemisphere European basins and could potentially open new location for the understanding of the palaeolclimatic fluctuation at the Triassic–Jurassic boundary.

Acknowledgments

The research is the outcome of the PhD study under the OSS-II/HEC, Pakistan. IGCP-609 support for the fieldwork and samples analyses is acknowledged. The authors are thankful to Mr. Hafiz Shahid Hussain, Mr. Mukhtiar Ghani and Mr. Syed Irfan Hashmi for their help during the fieldwork. Claudia Beybel, Ilka Wünsche and Leopold Slawek are thanked for their technical support in thin section preparation and Maria Meszar is thanked for her help in the clay mineralogy sample preparation. The comments and suggestions of the two anonymous reviewers have greatly improved the quality of the manuscript.

Appendix A. Supplementary data

Supplementary data to this article can be found online at https://doi.org/10.1016/j.gloplacha.2018.09.008.

References

Ahlberg, A., Olsson, I., Simkevicius, P., 2003. Triassic–Jurassic weathering and clay mineral dispersal in basement areas and sedimentary basins of southern Sweden. Sediment. Geol. 161, 15–29. https://doi.org/10.1016/S0037-0738(02)00381-0.

Allen, J.R.L., Hoskins, B.J., Sellwood, B.W., Spicer, R.S., Valdes, P.J. (Eds.), 1994. Palaeoclimates and their Modelling: With Special Reference to the Mesozoic Era. Chapman and Hall, pp. 140.

Anwar, M., Fatmi, A.M., Hyderi, I.H., 1992. Revised Nomenclature and Stratigraphy of Musakhel and Baroch Groups in Surghar Range, Pakistan. J. Geol. 15–28.

Arche, A., and López-Gómez, J. (2014) The Carnian Pluvial Event in Western Europe: new data from Iberia and correlation with the Western Neotethys and Eastern North America–NW Africa regions. Earth-Sci. Rev., 128, 196–231. https://doi.org/10.1016/j.earscirev.2013.10.012.

Arias, C., 2007. Pliensbachian–Toarcian ostracod biogeography in NW Europe: evidence for water mass structure evolution. Palaeogeogr. Palaeoclimatol. Palaeoecol. 251 (3), 398–421.

Bachan, A., van de Schootbrugge, B., Payne, J.L., 2014. The end-Triassic negative $\delta^{13}C$ excursion: a lithologic test. Palaeogeogr. Palaeoclimatol. Palaeoecol. 412, 177–186. https://doi.org/10.1016/j.palaeo.2014.07.027.

Bahlburg, H., Dobrzinski, N., 2011. A review of the Chemical Index of Alteration (CIA) and its application to the study of Neoproterozoic glacial deposits and climate transitions. Geol. Soc. Lon. Memoirs. 36 (1), 81–92. https://doi.org/10.1144/M36.6.

Baker, D.M., Lillie, R.J., Yeats, R.S., Johnson, G.D., Yousuf, M., Zamin, A.S.H., 1988. Development of the Himalayan frontal thrust zone: Salt Range. Pak. Geol. 16, 3–7.

Balog, A., Read, J.F., Haas, J., 1999. Climate-controlled early dolomite, Late Triassic cyclic platform carbonates, Hungary. J. Sediment. Res. 69 (1), 267–282.

Basu, A., 1976. Petrology of Holocene fluvial sand derived from plutonic source rocks: Implication to paleoclimatic interpretation. J. Sed. Petrol. 46, 694–709.

Beerling, D.J., Berner, R.A., 2002. Biogeochemical constraints on the Triassic–Jurassic boundary carbon cycle event. Glob. Biogeochem. Cycles 16 (3), 101–113. https://doi.org/10.1029/2001GB001637.

Blackburn, T.J., Olsen, P.E., Bowring, S.A., McLean, N.M., Kent, D.V., Puffer, J., McHone, G., Troy Rasbury, E., Et-Touhami, M., 2013. Zircon U-Pb geochronology links the end-Triassic extinction with the Central Atlantic Magmatic Province. Science 340, 941–945.

Blatt, H., 1982. Sedimentary Petrology. Freeman and Company, New York, pp. 105–241.

Boggs Jr., S., 2006. Principles of Sedimentology and Stratigraphy. Pearson Education, pp. 119–157.

Boggs Jr., S., 2009. Petrology of Sedimentary Rocks, 2nd edn. Cambridge University Press, pp. 166–193.

Bonis, N.R., Kürschner, W.M., 2012. Vegetation history, diversity patterns, and climate change across the Triassic/Jurassic boundary. Paleobiology 38, 240–264. https://doi.org/10.1666/09071.1.

Bonis, N.R., Ruhl, M., Kürschner, W.M., 2010. Climate change driven black shale deposition during the end-Triassic in the western Tethys. Palaeogeogr. Palaeoclimatol. Palaeoecol. 290, 151–159. https://doi.org/10.1016/j.palaeo.2009.06.016.

Breda, A., Preto, N., 2011. Anatomy of an Upper Triassic continental to marginal-marine system: the mixed siliciclastic-carbonate Travenanzes Formation (Dolomites, Northern Italy). Sedimentology 58, 1613–1647. https://doi.org/10.1111/j.1365-3091.2011.01227.x.

Brindley, G.W., Brown, G., 1980. Crystal Structures of Clay Minerals and Their X-ray Identification. Mineralogical Society, London, pp. 495.

Buggle, B., Glaser, B., Hambach, U., Gerasimenko, N., Marković, S., 2011. An evaluation of geochemical weathering indices in loess–paleosol studies. Quat. Int. 240 (1), 12–21. https://doi.org/10.1016/j.quaint.2010.07.019.

Burbank, D.W., Raynolds, R.G.H., 1988. Stratigraphic keys to the timing of thrusting in the terrestrial foreland basins: applications to the northwest Himalaya. In: Kleinspahn, K.L., Paol, C. (Eds.), Frontiers in Sedimentary Geology, New Perspective in Basin Analysis. Springer, Berlin, pp. 331–351.

Clemmensen, L.B., Kent, D.V., Jenkins, F.A., 1998. A Late Triassic lake system in East Greenland: facies, depositional cycles and palaeoclimate. Palaeogeo. Palaeoclimatol. Palaeoecol. 140 (1), 135–159 PII S0031–0 1 8 2 (9 8) 0 0 0 4 3–1.

Climap, P.M., 1976. The surface of the ice-age Earth. Science (New York, N.Y.) 191 (4232), 1131–1137.

Crowley, T.J., North, G.R., 1991. Paleoclimatology. Oxford University Press 349 pp.

Cullers, R.L., 2002. Implications of elemental concentrations for provenance, redox conditions, and metamorphic studies of shales and limestones near Pueblo, CO, USA. Chem. Geol. 191 (4), 305–327.

Dal Corso, J., Mietto, P., Newton, R.J., Pancost, R.D., Preto, N., Roghi, G., Wignall, P.B., 2012. Discovery of a major negative δ13C spike in the Carnian (Late Triassic) linked to the eruption of Wrangellia flood basalts. Geology 40, 79–82. https://doi.org/10.1130/G32473.1.

Damborenea, S.E., 2002. Jurassic evolution of Southern Hemisphere marine palaeobiogeographic units based on benthonic bivalves. Geobios, M'emoire Sp'ecial 35, 51–71.

Danilchik, W., 1961. The Iron formation of the Surghar and western Salt Range, Mianwali District, West Pakistan. U. S. Geol. Surv. 424-D, 228–231 Prof. Paper.

Danilchik, W., Shah, S.M.I., 1967. Stratigraphic nomenclature of formations in Trans-Indus Mountains, Mianwali District, West Pakistan. U. S. Geol. Surv. 1–45 Proj.

Report (IR) PK-33.
Davies, J.H.F.L., Marzoli, A., Bertrand, H., Youbi, N., Ernesto, M., Schaltegger, U., 2016. End-Triassic mass extinction started by intrusive CAMP activity. Nat. Comm. 8, 15596. https://doi.org/10.1038/ncomms15596.
Davis, D.M., Lillie, R.J., 1994. Changing mechanical response during continental collision: active examples from the foreland thrust belts of Pakistan. J. Struct. Geol. 16, 21–34.
De Caritat, P., Reimann, C., Team, N.P., Team, G.P., 2012. Comparing results from two continental geochemical surveys to world soil composition and deriving Predicted Empirical Global Soil (PEGS2) reference values. Earth Planet. Sci. Lett. 319, 269–276.
Dickinson, W.R., 1970. Interpreting detrital modes of graywacke and arkose. J. Sed. Petrol. 40, 695–707.
Dickinson, W.R., Suczek, C.A., 1979. Plate tectonics and sandstone compositions: Am. Assoc. Petr. Geol. Bull. 63, 2164–2182.
Dill, H.G., 2016. Kaolin: Soil, rock and ore: From the mineral to the magmatic, sedimentary and metamorphic environments. Earth Sci. Rev. 161, 16–129. https://doi.org/10.1016/j.earscirev.2016.07.003.
DiPietro, J.A., 1990. Stratigraphy, Structure, and Metamorphism near Saidu Sharif, Lower Swat, Pakistan. Ph.D. thesis. Oregon State Univ., Corvallis (182p).
Dipietro, J.A., Pogue, K.R., Hussain, A., Ahmad, I., 1999. Geologic map of the Indus syntaxis and surrounding area, northwest Himalaya, Pakistan. Spec. Pap.-Geol. Soc. Am. 159–178.
Dubiel, R.F., Parrish, J.T., Parrish, J.M., Good, S.C., 1991. The Pangean megamonsoon — evidence from the upper triassic chinle formation, Colorado Plateau. PALAIOS 6, 347–370. https://doi.org/10.2307/3514963.
Duncan, R.A., Hooper, P.R., Rehacek, J., Marsh, J.S., Duncan, A.R., 1997. The timing and duration of the Karoo igneous event, southern Gondwana. J. Geophys. Res. Solid Earth 102 (B8), 18127–18138.
Fatmi, A.N., 1977. Mesozoic. In: Shah, S.M.I. (Ed.), Stratigraphy of Pakistan. 12. pp. 29–44 GSP Mem.
Use of proxies in paleoceanography: examples from the South Atlantic. In: Fischer, G., Wefer, G. (Eds.), Springer Science & Business Media, pp. 1–735.
Frakes, L.A., 1979. Climates Throughout Geologic Time. Elsevier, Amsterdam 310 pp.
Frakes, L.A., Francis, J.E., Syktus, J.I., 1992. Climate Modes of the Phanerozoic. Cambridge 274 pp.
Frisia, S., Wenk, H.R., 1993. TEM and AEM study of pervasive, multi-step dolomitization of the upper Triassic Dolomia Principale (Northern Italy) J. Sed. Petrol. 63, 1049–1058.
Fürsich, F.T., Wilmsen, M., Seyed-Emami, K., Majidifard, M.R., 2009. Lithostratigraphy of the upper triassic–middle jurassic shemshak group of Northern Iran. Geol. Soc. Lond., Spec. Publ. 312 (1), 129–160. https://doi.org/10.1144/SP312.6.
Galli, M.T., Jadoul, F., Bernasconi, S.M., Weissert, H., 2005. Anomalies in global carbon cycling and extinction at the Triassic/Jurassic boundary: evidence from a marine C-isotope record. Palaeogeogr. Palaeoclimatol. Palaeoecol. 216 (3), 203–214. https://doi.org/10.1016/j.palaeo.2004.11.009.
Gazzi, P., 1966. Le arenarie del flysch sopracretaceo delrAppennino modenese; correlazioni con il flysch di Monghidoro. Mineralogica e Petrografica Acta 12, 69–97.
Gazzi, P., Zuffa, G.G., Gandolfi, G., Paganelli, L., 1973. Provenienza e dispersione litoranea delle sabbie delle spiagge adriatiche fra le foci delrlsonzo e del Foglia: inquadramento regionale. Memofie della Societa Geologica Italiana 12, 1–37.
Gee, E.R., 1945. The age of the saline series of the Punjab and of Kohat. Proc. Ind. Acad. Sci. Sect. B 14, 269–310.
Ghazi, S., Mountney, N.P., 2011. Petrography and provenance of the Early Permian fluvial Warchha Sandstone, Salt Range, Pakistan. Sediment. Geol. 233, 88–110.
Goldberg, K., Humayun, M., 2010. The applicability of the chemical index of alteration as a paleoclimatic indicator: an example from the Permian of the Paraná Basin, Brazil. Palaeogeogr. Palaeoclimatol. Palaeoecol. 293 (1), 175–183. https://doi.org/10.1016/j.palaeo.2010.05.015.
Graham, S.A., Ingersoll, R.V., Dickinson, W.R., 1976. Common provenance for lithic grains in carboniferous sandstones from ouachita mountains and Black Warrior basin. J. Sed. Petrol. 46, 620–632.
Greene, S.E., Martindale, R.C., Ritterbush, K.A., Bottjer, D.J., Corsetti, F.A., Berelson, W.M., 2012. Recognising ocean acidification in deep time: an evaluation of the evidence for acidification across the Triassic–Jurassic boundary. Earth Sci. Rev. 113 (1–2), 72–93. https://doi.org/10.1016/j.earscirev.2012.03.009.
Gromet, L.P., Haskin, L.A., Korotev, R.L., Dymek, R.F., 1984. The “North American shale composite”: its compilation, major and trace element characteristics. Geochim. Cosmochim. Acta 48 (12), 2469–2482.
Haas, J., Demény, A., 2002. Early dolomitisation of late triassic platform carbonates in the transdanubian range (Hungary). Sediment. Geol. 151 (3–4), 225–242.
Haas, J., Tardy-Filácz, E., 2004. Facies changes in the Triassic–Jurassic boundary interval in an intraplatform basin succession at Csővár (Transdanubian Range, Hungary). Sedimen. Geol. 168 (1), 19–48. https://doi.org/10.1016/j.sedgeo.2004.03.002.
Hallam, A., 1987. Radiations and extinctions in relation to environmental change in the marine Jurassic of north west Europe. Paleobiology 13, 152–168.
Hallam, A., 1988. A re-evaluation of the Jurassic eustasy in the light of new data and the revised Exxon curve. In: Wilgus, C.K., Hastings, B.S., Kendall, G.St.C., Posamentier, H.W., Ross, C.A., van Wagoner, J.C. (Eds.), Sea- Level Changes: An Integrated Approach. Society of Economic Paleontologists and Mineralogists, Special Publications. 42. pp. 71–108. https://doi.org/10.2110/sepmsp.105.
Hallam, A., 1997. Estimates of the amount and rate of sea-level change across the Rhaetian–Hettangian and Pliensbachian–Toarcian boundaries (latest Triassic to early Jurassic). J. Geol. Soc. 154, 773–779 London.
Hallam, A., 2001. A review of the broad pattern of Jurassic sea-level changes and their possible causes in the light of current knowledge. Palaeogeo. Palaeoclimatol. Palaeoecol. 167 (1), 23–37 PII: S0031-0182(00)00229–7.
Hallam, A., Maynard, J.B., 1987. The iron ores and associated sediments of the Chichali Formation (Oxfordian to Valanginian) of the Trans-Indus Salt Range, Pakistan. J. Geol. Soc. 44 (1), 107–114. https://doi.org/10.1144/gsjgs.144.1.0107.
Hallam, A., Wignall, P.B., 1999. Mass extinctions and sea-level changes. Earth-Sci. Rev. 48, 217–250 PII: S 0 0 1 2–8 2 5 2 9 9 0 0 0 5 5–0.
Han, W., Hong, H.L., Yin, K., Churchman, G.J., Li, Z.H., Chen, T., 2014. Pedogenic alteration of illite in subtropical China. Clay Miner. 49 (3), 379–390. https://doi.org/10.1180/claymin.2014.049.3.03.
Hanif, M., Imraz, M., Ali, F., Haneef, M., Saboor, A., Iqbal, S., Ahmad Jr., S., 2014. The inner ramp facies of the Thanetian Lockhart Formation, western Salt Range, Indus Basin, Pakistan. Arab. J. Geosci. 7 (11), 4911–4926. https://doi.org/10.1007/s12517-013-1099-7.
Haq, B.U., 2017. Jurassic Sea-Level Variations: A Reappraisal. GSA Today 28 (1). https://doi.org/10.1130/GSATG359A.1.
Haq, B.U., Hardenbol, J., Vail, P.R., 1987. The chronology of fluctuating sea level since the Triassic. Science 235, 1156–1167. https://doi.org/10.1126/science.235.4793.1156.
Harrison, J.L., Greenberg, S.S., 1998. Dehydration of fully hydrated halloysite from Lawrence County. Indiana 374–377.
Harvey, C., Murray, H., 1990. The geology, mineralogy and exploitation of halloysite clays of Northland, New Zealand. In: Keller (Ed.), Kaolin Symposium, Kaolin Genesis and Utilization. Publication Clay Mineral Society, pp. 233–248.
Hesselbo, S.P., Gröcke, D.R., Jenkyns, H.C., Bjerrum, C.J., Farrimond, P., Morgans Bell, H.S., Green, O.R., 2000. Massive dissociation of gas hydrate during a Jurassic oceanic anoxic event. Nature 406, 392–395. https://doi.org/10.1038/35019044.
Hesselbo, S.P., Robinson, S.A., Surlyk, F., Piasecki, S., 2002. Terrestrial and marine extinction at the Triassic–Jurassic boundary synchronized with major carbon-cycle perturbation: a link to initiation of massive volcanism? Geology 30, 251–254.
Hesselbo, S.P., Robinson, S.A., Surlyk, F., 2004. Sea-level change and facies development across potential Triassic–Jurassic boundary horizons, SW Britain. J. Geol. Soc. 161 (3), 365–379.
Hillebrandt, A.V., Krystyn, L., Kürschner, W.M., Bonis, N.R., Ruhl, M., Richoz, S., Schobben, M.A.N., Urlichs, M., Bown, P.R., Kment, K., McRoberts, C.A., 2013. The global stratotype sections and point (GSSP) for the base of the Jurassic System at Kuhjoch (Karwendel Mountains, Northern Calcareous Alps, Tyrol, Austria). Episodes 36 (3), 162–198.
Hofmann, P., Ricken, W., Schwark, L., Leythaeuser, D., 2001. Geochemical signature and related climatic-oceanographic processes for early Albian black shales: Site 417D, North Atlantic Ocean. Cretac. Res. 22 (2), 243–257. https://doi.org/10.1006/cres.2001.0253.
Hornung, T., Krystyn, L., Brandner, R., 2007. A Tethys-wide mid-Carnian (Upper Triassic) carbonate productivity decline: evidence for the Alpine Reingraben Event from Spiti (Indian Himalaya). J. Asian Earth Sci. 30, 230–285. https://doi.org/10.1016/j.jseaes.2006.10.001.
Huber, B.T., MacLeod, K.G., Wing, S.T. (Eds.), 2000. Warm Climates in Earth History. Cambridge University Press 462 pp.
Iannace, A., Frisia, S., 1994. Changing dolomitization styles from Norian to Rhaetian in southern Tethys realm. In: Purser, B., Tucker, M., Zenger, D. (Eds.), A Volume in Honour of Dolomieu 21. Int. Assoc. Sedimentol. Spec. Publ, pp. 75–89.
Ingersoll, R.V., Bullard, T.F., Ford, R.L., Grimm, J.P., Pickle, J.D., Sares, S.W., 1984. The effect of grain size on detrital modes: a test of the Gazzi-Dickinson point-counting method. J. Sediment. Res. 54 (1), 103–116.
Iqbal, S., Wagreich, M., 2016. Evidences of marine regression and Pangaea breakup: Triassic-Jurassic boundary from the Tethyan Salt Range, Pakistan. (35th IGC Capetown South Africa Paper Number: 1979).
Iqbal, S., Jan, U.I., Hanif, M., 2014. The Mianwali and Tredian Formations: an example of the Triassic Progradational Deltaic System in the low-latitude western Salt Range, Pakistan. Arab. J. Sci. Eng. 39 (7), 5489–5507. https://doi.org/10.1007/s13369-013-0836-2.
Iqbal, S., Akhter, G., Bibi, S., 2015a. Structural model of the Balkassar area, Potwar Plateau, Pakistan. Int. J. Earth Sci. 104 (8), 2253–2272. https://doi.org/10.1007/s00531-015-1180-4.
Iqbal, S., Jan, I.U., Akhter, M.G., Bibi, M., 2015b. Palaeoenvironmental and sequence stratigraphic analyses of the Jurassic Datta Formation, Salt Range, Pakistan. J. Earth Sys. Sci. 124 (4), 747–766. https://doi.org/10.1007/s12040-015-0572-y.
Iqbal, S., Wagreich, M., Jan, I., Kürschner, W.M., Gier, S., 2017. Geochemical evidences for palaeoclimatic fluctuations at the Triassic-Jurassic boundary: southwestern margin of the Neotethys in the Salt Range, Pakistan. In: EGU General Assembly Conference Abstracts. 19. pp. 408.
Jacobs, D.K., Sahagian, D.L., 1993. Climate induced fluctuations in sea level during nonglacial times. Nature 361, 710–712.
Jadoon, I.A.K., Kemal, A., Frisch, W., Jaswal, T.M., 1997. Thrust geometries and kinematics in the Himalayan foreland (North Potwar Deformed Zone), North Pakistan. Geol. Rundsch. 86, 120–131.
Jain, A.K., 2014. When did India–Asia collide and make the Himalaya? Curr. Sci. 106 (2), 254–266.
Jan, I.U., Iqbal, S., Davies, S.J., Zalasiewicz, J.A., Stephenson, M.H., Wagreich, M., Haneef, M., Hanif, M., Ahmad, S., 2017. A periglacial palaeoenvionment in the upper carboniferous–lower permian tobra formation of the salt range, Pakistan. Acta Geol. Sin. Engl. Ed. 91 (3), 1063–1078.
Jenkyns, H.C., 1988. The early Toarcian (Jurassic) anoxic event: stratigraphic, sedimentary and geochemical evidence. Am. J. Sci. 288, 101–151.
Jenkyns, H.C., 1999. Mesozoic anoxic events and palaeoclimate. Zentralbl. Geol. Palaeontol. 1 (7–9), 943–949.
Kadri, I.B., 1995. Petroleum Geology of Pakistan. Pakistan Petroleum Limited, Karachi Pak, pp. 40–61.

Kazmi, A.H., Jan, M.Q., 1997. Geology and Tectonic of Pakistan. Graphic publication, Karachi, pp. 130–141.
Keller, W.D., Westcott, J.F., Bledsoe, A.O., 1954. The origin of Missouri fire clays. In: 2nd National Conference on Clays and Clay Minerals, pp. 7–46.
Kent, D.V., Olsen, P.E., 2000. Magnetic polarity stratigraphy and paleolatitude of the Triassic Jurassic Blomidon Formation in the Fundy basin (Canada): implications for early Mesozoic tropical climate gradients. Earth Planet. Sci. Lett. 179, 311–324. https://doi.org/10.1016/S0012-821X(00)00117-5.
Kidder, D.L., Worsley, T.R., 2010. Phanerozoic large igneous provinces (LIPs), HEATT (haline euxinic acidic thermal transgression) episodes, and mass extinctions. Palaeogeogr. Palaeoclimatol. Palaeoecol. 295 (1), 162–191. https://doi.org/10.1016/j.palaeo.2010.05.036.
Klett, T.R., Ulmishek, G.F., Wandrey, C.J., Agena, W.F., 2006. Assessment of undiscovered technically recoverable conventional petroleum resources of northern Afghanistan. US Geol. Sur. Open-File Rep. 2006, 1253.
Korte, C., Hesselbo, S.P., Jenkins, H.C., Rickaby, R.E.M., Spotl, C., 2009. Palaeoenvironmental significance of carbon- and oxygen-isotope stratigraphy of marine Triassic–Jurassic boundary sections in SW Britain. J. Geol. Soc. 166, 431–445. https://doi.org/10.1144/0016-76492007-177.
Kuerschner, W.M., Bonis, N.R., Krystyn, L., 2007. Carbon-isotope stratigraphy and palynostratigraphy of the Triassic–Jurassic transition in the Tiefengraben section—Northern Calcareous Alps (Austria). Palaeogeogr. Palaeoclimatol. Palaeoecol. 244 (1), 257–280. https://doi.org/10.1016/j.palaeo.2006.06.031.
Kuerschner, W.M., Iqbal, S., Wagreich, M., Jan, I., Gier, S., 2017. Palynology and Carbon isotope stratigraphy of the Triassic-Jurassic transition in the Salt Range (Pakistan). In: EGU General Assembly Conference Abstracts. Vol. 19. pp. 15291.
Kutzbach, J.E., Gallimore, R.G., 1989. Pangaean climates: megamonsoons of the megacontinent. J. Geophys. Res. 94, 3341–3358. https://doi.org/10.1029/JD094iD03p03341.
Van Langeveld, A. D., Van der Gaast, S. J., and Eisma, D. (1978) Comparison of the effectiveness of eight methods for the removal of organic matter from clay. Clay Clay Miner., 26(5), 361–4.
Letourneau, P.M., Huber, P., 2006. Early Jurassic eolian dune field, Pomperaug basin, Connecticut and related synrift deposits: Stratigraphic framework and paleoclimatic context. Sediment. Geol. 187 (1), 63–81. https://doi.org/10.1016/j.sedgeo.2005.12.005.
Lindström, S., van de Schootbrugge, B., Hansen, K.H., Pedersen, G.K., Alsen, P., Thibault, N., Dybkjær, K., Bjerrum, C.J., Nielsen, L.H., 2017. A new correlation of Triassic–Jurassic boundary successions in NW Europe, Nevada and Peru, and the Central Atlantic Magmatic Province: A time-line for the end-Triassic mass extinction. Palaeogeogr. Palaeoclimatol. Palaeoecol. 478, 80–102.
López-Gómez, J., Escudero-Mozo, M.J., Martín-Chivelet, J., Arche, A., Lago, M., Galé, C., 2017. Western Tethys continental-marine responses to the Carnian Humid Episode: Palaeoclimatic and palaeogeographic implications. Glob. Planet. Chang. 148, 79–95. https://doi.org/10.1016/j.gloplacha.2016.11.016.
Luo, M., Chen, Z.Q., Shi, G.R., Fang, Y., Song, H., Jia, Z., Huang, Y., Yang, H., 2016. Upper Lower Triassic stromatolite from Anhui, South China: geobiologic features and paleoenvironmental implications. Palaeogeogr. Palaeoclimatol. Palaeoecol. 452, 40–54. https://doi.org/10.1016/j.palaeo.2016.04.008.
Malick, B.M.L., Ishiga, H., 2016. Geochemical classification and determination of maturity source weathering in beach sands of Eastern San'in Coast, Tango Peninsula, and Wakasa Bay, Japan. Earth Sci. Res. 5 (1), 44. https://doi.org/10.5539/esr.v5n1p44.
Martin, A.J., 2017. A review of Himalayan stratigraphy, magmatism, and structure. Gondwana Res. 49, 42–80. https://doi.org/10.1016/j.gr.2017.04.031.
Marzoli, A., Renne, P.R., Piccirillo, E.M., Ernesto, A., Bellieni, G., De Min, A., 1999. Extensive 200-million-year-old continental flood basalts of the Central Atlantic magmatic province. Science 284, 616–618.
Marzoli, A., Bertrand, H., Knight, K.B., Cirilli, S., Buratti, N., Ve'rati, C., Nomade, S., Renne, P.R., Youbi, N., Martini, R., Allenbach, K., Neuwerth, R., Rapaille, C., Zaninetti, L., Bellieni, G., 2004. Synchrony of the Central Atlantic magmatic province and the Triassic-Jurassic boundary climatic and biotic crisis. Geology 32, 973–976. https://doi.org/10.1130/G20652.1.
Marzoli, A., Jourdan, F., Puffer, J.H., Cuppone, T., Tanner, L.H., Weems, R.E., Bertrand, H., irilli, S., Bellieni, G., De Min, A., 2011. Timing and duration of the Central Atlantic magmatic province in the Newark and Culpeper basins, eastern USA. Lithos 122 (3), 175–188.
McElwain, J.C., Beerling, D.J., Woodward, F.I., 1999. Fossil plants and global warming at the Triassic–Jurassic boundary. Science 285, 1386–1390. https://doi.org/10.1126/science.285.5432.1386.
McElwain, J. C., Popa, M. E., Hesselbo, S. P., Haworth, M., and Surlyk, F., (2007) Macroecological response of terrestrial vegetation to climatic and atmospheric change across the Triassic/Jurassic boundary in East Greenland. Paleobiology 33, 547–573. 10.1666/06026.1
McLennan, S.M., Hemming, S., McDaniel, D.K., Hanson, G.M., 1993. Geochemical approaches to sedimentation. provenance, and tectonics. In: Johnsson, M.J., Basu, A. (Eds.), Processes Controlling the Composition of Clastic Sediments. Geological Society of America, Special Papers 284, 21–40. https://doi.org/10.1130/SPE284-p21.
Meister, P., McKenzie, J.A., Bernasconi, S.M., Brack, P., 2013. Dolomite formation in the shallow seas of the Alpine Triassic. Sedimentology 60, 270–291. https://doi.org/10.1111/sed.12001.
Meyen, S.V., 1997. Permian conifers of western Angaraland. Rev. Palaeobot. Palynol. 96, 351–447. https://doi.org/10.1016/S0034-6667(96)00046-2.
Michalik, J., Biron, A., Lintnerova, O., Gotz, A.E., Ruckwied, K., 2010. Climate change at the Triassic/Jurassic boundary in the northwestern Tethyan realm, inferred from sections in the Tatra Mountains (Slovakia). Acta Geol. Pol. 60 (4), 535–548.
Michalik, J., Lintnerová, O., Wójcik-Tabol, P., Gaździcki, A., Grabowski, J., Golej, M., Šimo, V., Zahradníková, B., 2013. Paleoenvironments during the Rhaetian transgression and the colonization history of marine biota in the Fatric Unit (Western Carpathians). Geol. Carpath. 64 (1), 39–62. https://doi.org/10.2478/geoca-2013-0003.
Mikutta, R., Kleber, M., Kaiser, K., Jahn, R., 2005. Review. Soil Sci. Soc. Am. J. 69 (1), 120–135. https://doi.org/10.2136/sssaj2005.0120.
Mindszenty, A., 2016. Bauxites: Feedbacks of System Earth at Greenhouse times. Geologia Croatica 69 (1), 79–87. https://doi.org/10.4154/gc.2016.07.
Mohadjer, S., Bendick, R., Ischuk, A., Kuzikov, S., Kostuk, A., Saydullaev, U., Lodi, S., Kakar, D. M., Wasy, A., Khan, M. A., Molnar, P., Bilham, R., and Zubovich, A. V., (2010) Partitioning of India-Eurasia convergence in the Pamir-Hindu Kush from GPS measurements. Geophys. Res. Lett. 37:L04305. doi:https://doi.org/10.1029/2009GL041737.
Molnar, P., Tapponnier, P., 1981. A possible dependence of tectonic strength on the age of the crust in Asia. Earth Planet. Sci. Lett. 52, 107–114.
Moore, D., and Reynolds, R.C. Jr. (1997) X-Ray Diffraction and the Identification and Analysis of Clay Minerals, second ed.: Oxford University Press, New York, Vol. 378 p.
Mount, J.F., 1984. Mixing of siliciclastic and carbonate sediments in shallow shelf environments. Geology 12 (7), 432–435.
Mukhopadhyay, G., Mukhopadhyay, S.K., Roychowdhury, M., Parui, P.K., 2010. Stratigraphic correlation between different Gondwana basins of India. J. Geol. Soc. India 76 (3), 251–266.
Nesbitt, H.W., Young, G.M., 1982. Early Proterozoic climates and plate motions inferred from major element chemistry of lutites. Nature 299, 715–717.
Nesbitt, H.W., Young, G.M., 1984. Prediction of some weathering trends of plutonic and volcanic rocks based on thermodynamic and kinetic considerations. Geochim. Cosmochim. Acta 48, 1523–1534.
Nesbitt, H.W., Young, G.M., 1989. Formation and diagenesis of weathering profiles. J. Geol. 97, 129e–147. https://doi.org/10.1086/629290.
Nesbitt, H.W., Young, G.M., McLennan, S.M., Keays, R.R., 1996. Effects of chemical weathering and sorting on the petrogenesis of siliciclastic sediments, with implications for provenance studies. J. Geol. 104 (5), 525–542.
Nichols, G., 2000. Sedimentology and stratigraphy, Blackwell Science. pp. 75–145.
Nichols, G., 2009. Sedimentology and stratigraphy. John Wiley & Sons, pp. 90–133.
Olsen, P.E., 1999. Giant lava flows, mass extinctions, and mantle plumes. Science. https://doi.org/10.1126/science.284.5414.604.
Olsen, P.E., Kent, D.V., 1996. Milankovitch climate forcing in the tropics of Pangea during the Late Triassic. Palaeogeogr. Palaeoclimatol. Palaeoecol. 122, 1–26.
Olsen, P.E., Kent, D.V., 2000. High resolution early Mesozoic Pangean climatic transect in lacustrine environments. Zbl. Geol. Paläontol. 11–12, 1475–1496 0340-5109/00/1998-147.
Pálfy, J., Smith, P.L., 2000. Synchrony between Early Jurassic extinction, oceanic anoxic event, and the Karoo–Ferrar flood basalt volcanism. Geology 28, 747–750.
Pálfy, J., Zajzon, N., 2012. Environmental changes across the Triassic–Jurassic boundary and coeval volcanism inferred from elemental geochemistry and mineralogy in the Kendlbachgraben section (Northern Calcareous Alps, Austria). Earth Planet. Sci. Lett. 335–336, 121–134. https://doi.org/10.1016/j.epsl.2012.01.039.
Pálfy, J., Parrish, R.R., Smith, P.L., 1997. A U–Pb age from the Toarcian (Lower Jurassic) and its use for time scale calibration through error analysis of biochronologic dating. Earth Planet. Sci. Lett. 146, 659–675 (PII S0012-821X 96 00241-5).
Pálfy, J., Mortensen, J.K., Carter, E.S., Smith, P.L., Friedman, R.M., Tipper, H.W., 2000. Timing of the end Triassic mass extinction: first on land, then in sea? Geology 28, 39–42.
Pálfy, J., Deme'ny, A., Haas, J., Hete'nyi, M., Orchard, M.J., Veti, I., 2001. Carbon isotope anomaly and other geochemical changes at the Triassic–Jurassic boundary from a marine section in Hungary. Geology 29, 1047–1050.
Parrish, J.T., 1993. Climate of the supercontinent Pangea. J. Geol. 101, 215–233.
Pettijohn, F.J., Potter, P.E., 1987. In: Siever, R. (Ed.), Sand and Sandstone, 2nd edition. Springer Verlag, pp. 533.
Pieńkowski, G., Niedźwiedzki, G., Waksmundzka, M., 2012. Sedimentological, palynological and geochemical studies of the terrestrial Triassic–Jurassic boundary in northwestern Poland. Geol. Mag. 149 (02), 308–332. https://doi.org/10.1017/S0016756811000914.
Pogue, K.R., Dipietro, J.A., Khan, S.R., Hughes, S.S., Dilles, J.H., Lawrence, R.D., 1992. Late Paleozoic rifting in northern Pakistan. Tectonics 11 (4), 871–883. https://doi.org/10.1029/92TC00335.
Polyak, V.W.C., Guven, N., 1996. Alunite, natroalunite, and hydrated halloysite in Carlsbad Cavern. Clay Miner. 44, 843–850.
Poulsen, C.J., 2009. Paleoclimate modeling, pre-quaternary. In: Encyclopedia of Paleoclimatology and Ancient Environments. Springer, Netherlands, pp. 700–709.
Preto, N., Kustatscher, E., Wignall, P., 2010. Triassic climates—state of art. Palaeogeogr. Palaeoclimatol. Palaeoecol. 290, 1–10. https://doi.org/10.1016/j.palaeo.2010.03.015.
Preto, N., Breda, A., Dal Corso, J., Spötl, C., Zorzi, F., Frisia, S., 2015. Primary dolomite in the Late Triassic Travenanzes Formation, Dolomites, Northern Italy: facies control and possible bacterial influence. Sedimentology 62 (3), 697–716. https://doi.org/10.1111/sed.12157.
Raup, D.M., Sepkoski Jr., J.J., 1982. Mass extinction in the marine fossil record. Science 215, 1501–1503.
Reading, H.G. (Ed.), 2009. Sedimentary Environments: Processes, Facies and Stratigraphy. John Wiley & Sons.
Rees, P.M., Gibbs, M.T., Ziegler, A.M., Kutzbach, J.E., Behling, P.J., 1999. Permian climates: Evaluating model predictions using global paleobotanical data. Geology 27, 891–894.
Rees, P.M., Ziegler, A.M., Gibbs, M.T., Kutzbach, J.E., Behling, P.J., Rowley, D.B., 2002.

Permian phytogeographic patterns and climate data/model comparisons. J. Geol. 110, 1–31.
Rees, P.M., Ziegler, A.M., Valdes, P.J., 2000. Jurassic phytogeography and climates: new data and model comparisons. In: Huber, B.T., Macleod, K.G., Wing, S.L. (Eds.), Warm climates in Earth history. Cambridge University Press, pp. 297–318.
Retallack, G.J., 2010. Lateritization and Bauxitization Events. Econ. Geol. 105, 655–667. https://doi.org/10.2113/gsecongeo.105.3.655.
Roser, B.P., Korsch, R.J., 1988. Provenance signatures of sandstone-mudstone suites determined using discriminant function analysis of major-element data. Chem. Geol. 67 (1–2), 119–139. https://doi.org/10.1016/0009-2541(88)90010-1.
Ruckwied, K., Götz, A., 2009. Climate change at the Triassic/Jurassic boundary: palynological evidence from the Furkaska section (Tatra Mountains, Slovakia). Geol. Carpath. 60 (2), 139–149. https://doi.org/10.2478/v10096-009-0009-0.
Rudnick, R.L., Gao, S., 2003. Composition of the continental crust. In: Treatise on Geochemistry. 3. pp. 659.
Ruffell, A., Simms, M.J., Wignall, P.B., 2016. The Carnian Humid Episode of the late Triassic: a review. Geol. Mag. 153 (02), 271–284. https://doi.org/10.1017/S0016756815000424.
Ruhl, M., Kürschner, W.M., Krystyn, L., 2009. Triassic-Jurassic organic carbon isotope stratigraphy of key sections in the western Tethys realm (Austria). Earth Planet. Sci. Lett. 281, 169–187. https://doi.org/10.1016/j.epsl.2009.02.020.
Ruhl, M., Bonis, N.R., Reichart, G.-J., Sinninghe-Damsté, J.S., Kürschner, W.M., 2011a. Atmospheric Carbon injection linked to end-Triassic mass extinction. Science 333, 430–434. https://doi.org/10.1126/science.1204255.
Ruhl, M., Bonis, N.R., Reichart, G.J., Damsté, J.S.S., Kuerschner, W.M., 2011b. Atmospheric carbon injection linked to end-Triassic mass extinction. Science 333 (6041), 430–434. https://doi.org/10.1126/science.1204255.
Sa'ad, Z.A., Al-Mashaikie, Kedar, 2017. Tectonostratigraphic study of carbonate breccias (Calciturbidites) in the upper triassic baluti formation (Northern Iraq): new insights on tethyan geodynamics. In: Lithosphere Dynamics and Sedimentary Basins of the Arabian Plate and Surrounding Areas. Springer International Publishing, pp. 67–86.
Schaller, M.F., Wright, J.D., Kent, D.V., 2011. Atmospheric PCO_2 perturbations associated with the Central Atlantic Magmatic Province. Science 331, 1404–1409.
Schettino, A., Turco, E., 2011. Tectonic history of the western Tethys since the Late Triassic. Geol. Soc. Am. Bull. 123, 89–105.
Schoene, B., Guex, J., Bartolini, A., Schaltegger, U., Blackburn, T.J., 2010. Correlating the end-Triassic mass extinction and flood basalt volcanism at the 100 ka level. Geology 38, 387–390. https://doi.org/10.1130/G30683.1.
Schultz, L.G., 1964. Quantitative interpretation of mineralogical composition from X-ray and chemical data for the Pierre shale. US Geological Survey Prof. Paper 391-C. Washington.
Selley, C.R., 2000. Applied Sedimentology: 2nd Ed. Academic Press, pp. 182–207.
Sellwood, B.W., Valdes, P.J., 2006. Mesozoic climates: General circulation models and the rock record. Sediment. Geol. 190 (1), 269–287. https://doi.org/10.1016/j.sedgeo.2006.05.013.
Selvaraj, K., Chen, C.T.A., 2006. Moderate chemical weathering of subtropical Taiwan: constraints from solid-phase geochemistry of sediments and sedimentary rocks. J. Geol. 114 (1), 101–116 DOI:0022-1376/2006/11401-0006.
Selvaraj, K., Ram Mohan, V., Szefer, P., 2004. Evaluation of metal contamination in coastal sediments of the Bay of Bengal, India: geochemical and statistical approaches. Mar. Pollut. Bull. 49, 174–185.
Shah, S.M.I., 2009. Stratigraphy of Pakistan. Gov Pak Ministry of Petrol Nat Resour Geol Sur Pak, pp. 245–273.
Simms, M.J., Ruffell, A.H., 1989. Synchroneity of climatic change and extinctions in the Late Triassic. Geology 17 (3), 265–268.
Singer, A., 1984. The paleoclimatic interpretation of clay minerals in sediments—a review. Earth Sci. Rev. 21 (4), 251–293. https://doi.org/10.1016/0012-8252(84)90055-2.
Smoot, J.P., Olsen, P.E., 1988. Massive mudstones in basin analysis and paleoclimatic interpretation of the Newark Supergroup. In: Manspeizer, W. (Ed.), Triassic–Jurassic Rifting, Continental Breakup and the Origin of the Atlantic Ocean and Passive Margins. Elsevier, New York, pp. 249–274.
Song, E., Zhang, K., Chen, J., Wang, C., Jiang, G., Yin, K., Hong, H., Churchman, J.G., 2014. Clay Mineralogy and its Paleoclimatic Significance of the Oligocene-Miocene Sediments in the Gerze Basin, Tibet. Acta Geologica Sinica (English Edition) 7–23. https://doi.org/10.1111/1755-6724.12320.
Suttner, L.J., Dutta, P.K., 1986. Alluvial sandstone composition and paleoclimate, I. Framework mineralogy. J. Sediment. Res. 56 (3), 329–345.
Taylor, S.R., McLennan, S.M., 1985. The Continental Crust: Its Composition and Evolution. Blackwell, Oxford, pp. 312 ISBN-13: 978–0632011483.
Therrien, F., Fastovsky, D.E., 2000. Paleoenvironments of early theropods, chinle formation (Late Triassic), petrified forest National Park, Arizona. PALAIOS 15 (3), 194–211.
Thiry, M., 2000. Palaeoclimatic interpretation of clay minerals in marine deposits: an outlook from the continental origin. Earth Sci. Rev. 49 (1), 201–221. https://doi.org/10.1016/S0012-8252(99)00054-9.
Tucker, M.E. (Ed.), 2009. Sedimentary Petrology: An Introduction to the Origin of Sedimentary Rocks. John Wiley & Sons.
Valdes, P.J., Spicer, R.A., Sellwood, B.W., Palmer, D.C., 1999. Understanding Past Climates: Modelling Ancient Weather. (Routledge. CD-ROM).
Van de Schootbrugge, B., Quan, T.M., Lindström, S., Püttmann, W., Heunisch, C., Pross, J., Fiebig, J., Petschick, R., Röhling, H.G., Richoz, S., Rosenthal, Y., Falkowski, P.G., 2009. Floral changes across the Triassic/Jurassic boundary linked to flood basalt volcanism. Nat. Geosci. 2 (8), 589–594. https://doi.org/10.1038/ngeo577.
Wang, P.X., 2009. Global monsoon in a geological perspective. Chin. Sci. Bull. 54, 1113–1136. https://doi.org/10.1007/s11434-009-0169-4.
Weaver, C.E., 1958. A discussion on the origin of clay minerals in sedimentary rocks. In: Proc. 5th Natl. Conf.Clay and Clay Minerals, pp. 159–173.
Wefer, G., Berger, W.H., Bijma, J., Fischer, G., 1999. Clues to ocean history: a brief overview of proxies. In: Use of proxies in paleoceanography. Springer, Berlin Heidelberg, pp. 1–68.
Whitehouse, U.G., Jeffrey, L.M., Debrecht, J.D., 1960. Differential settling tendencies of clay minerals in artificial sea water. In: Proc. 7th Natl. Conf., Clays and Clay Minerals, pp. 1–80.
Whiteside, J. H., Grogana, D. S., Olsenb, P. E., and Kent, D. V., (2011) Climatically driven biogeographic provinces of Late Triassic tropical Pangea. PNAS, 108(22), 8972–8977. https://doi.org/10.1073/pnas.1102473108.
Wignall, P.B., 2001. Large igneous provinces and mass extinctions. Earth-Sci. Rev. 53, 1–33 PII: S0012–8252Ž00.00037–4.
Wilmsen, M., Fürsich, F.T., Seyed-Emami, K., Majidifard, M.R., 2009. An overview of the stratigraphy and facies development of the Jurassic System on the Tabas Block, east-central Iran. Geol. Soc. Lond., Spec. Publ. 312 (1), 323–343. https://doi.org/10.1144/SP312.15.
Wood, L.J., 1990. Effects of basin type on coastal plain shelf slope systems during base level fluctuations: an experimental approach. Am. Assoc. Petrol. Geol. Bull. 75, 969.
Worden, R.H., Burley, S.D., 2003. Sandstone diagenesis: the evolution of sand to stone. In: Sandstone Diagenesis: Recent and Ancient. Vol. 4. pp. 3–44.
Yan, D., Chen, D., Wang, Q., Wang, J., 2010. Large-scale climatic fluctuations in the latest Ordovician on the Yangtze block, south China. Geology 38, 599–602. https://doi.org/10.1130/G30961.1.
Zachos, J., Pagani, M., Sloan, L., Thomas, E., Billups, K., 2001. Trends, rhythms, and aberrations in global climate 65 Ma to present. Science 292 (5517), 686–693.
Ziegler, A.M., Scotese, C.R., Barrett, S.F., 1983. Mesozoic and Cenozoic paleogeographic maps, Tidal Friction and the Earth's Rotation, 2nd edition. Springer-Verlag, Berlin, pp. 240–252.
Ziegler, A.M., Eshet, G., McAllister Rees, P., Rothfus, T.A., Rowley, D.B., Sunderlin, D., 2003. Tracing the tropics across land and sea: Permian to present. Lethaia 36, 227–254. https://doi.org/10.1080/00241160310004657.